https://doi.org/10.5194/bg-2020-487
Preprint. Discussion started: 4 January 2021


Biogeosciences Discussions
Open Access
EGU

# Controls of ocean carbon cycle feedbacks from different ocean basins and meridional overturning in CMIP6

Anna Katavouta[1,2] and Richard G. Williams[1]

[1]Department of Earth, Ocean and Ecological Sciences, School of Environmental Sciences, University of Liverpool,Liverpool, UK
[2]National Oceanography Centre, Liverpool, UK

**Correspondence:** Anna Katavouta (a.katavouta@liverpool.ac.uk)

**Abstract.** The ocean response to carbon emissions involves a competition between the increase in atmospheric $CO_2$ acting to enhance the ocean carbon storage, characterised by the carbon-concentration feedback, and climate change acting to decrease the ocean carbon storage, characterised by the carbon-climate feedback. The contribution from different ocean basins to the carbon cycle feedbacks and its control by the ocean carbonate chemistry, physical ventilation and biological processes is explored in diagnostics of 10 CMIP6 Earth system models. To gain mechanist insight, the dependence of these feedbacks to the Atlantic Meridional Overturning Circulation (AMOC) is also investigated in an idealised climate model and the CMIP6 models. The Atlantic, Pacific and Southern Oceans contribute equally to the carbon-concentration feedback, despite their different size. This large contribution from the Atlantic Ocean relative to its size is associated with an enhanced carbon storage in the ocean interior due to a strong local physical ventilation and an influx of carbon transported from the Southern Ocean. The Atlantic Ocean provides the largest contribution to the carbon-climate feedback relative to its size, which is primarily due to climate change acting to reduce the physical ventilation. The Southern Ocean provides a relatively small contribution to the carbon-climate feedback, due to a compensation between the climate effects of the combined decrease in solubility and physical ventilation, and the increase in accumulation of regenerated carbon in the ocean interior. In the Atlantic Ocean, the AMOC strength and its weakening with warming has a strong control on the carbon cycle feedbacks that leads to a moderate dependence of these feedbacks to AMOC on global scale. In the Pacific, Indian and Southern Oceans there is no clear correlation between AMOC and the carbon cycle feedbacks, suggesting that other processes control the ocean ventilation and carbon storage there.

## 1 Introduction

Carbon emissions drive an Earth system response via direct changes in the biogeochemical carbon cycle and the physical climate. These changes in the biogeochemical carbon cycle and physical climate further amplify or dampen the Earth system response, with this indirect effect often refer to as a feedback (Sherwood et al., 2015). The physical climate feedback involves the combined effect from changes in atmospheric water vapour, lapse rate, surface albedo and clouds (Ceppi and Gregory, 2017), and from a shift in the regional patterns of ocean heat uptake due to changes in the ocean circulation (Winton et al., 2013). For the carbon cycle, an initial increase in atmospheric $CO_2$ leads to a carbon uptake and storage in land and ocean.

https://doi.org/10.5194/bg-2020-487
Preprint. Discussion started: 4 January 2021


Biogeosciences Discussions

At the same time, the carbon cycle is further modified by changes in the physical climate such that, for example, warming and an increase in ocean stratification lead to an amplification of the initial increase in atmospheric $CO_2$. These atmospheric $CO_2$ and climate-driven effects referred to as carbon-concentration and carbon-climate feedbacks, respectively, and have been extensively used to understand and quantify the response of the global carbon cycle to carbon emissions (Friedlingstein et al., 2003, 2006; Gregory et al., 2009; Boer and Arora, 2009; Arora et al., 2013; Schwinger et al., 2014; Schwinger and Tjiputra, 2018; Williams et al., 2019; Arora et al., 2020). A regional extension of the carbon cycle feedbacks have been also used to explore their geographical distribution and the mechanisms that control the land and ocean carbon uptake and storage in difference regions (Yoshikawa et al., 2008; Boer and Arora, 2010; Tjiputra et al., 2010; Roy et al., 2011).

On a global scale, the carbon-concentration feedback is of comparable strength over the land and ocean, while the carbon-climate feedback is about 3 times stronger over land than the ocean on centennial timescales in the CMIP6 Earth system modes (Arora et al., 2020). However, there is a substantial geographical variation in the carbon-climate feedback over the ocean (Tjiputra et al., 2010; Roy et al., 2011) as a result of an interplay between the effect of carbonate chemistry, physical ventilation and biological processes. In the tropics, the carbonate chemistry and the decrease in solubility with warming drives a reduction in the ocean carbon uptake with climate change (Roy et al., 2011; Rodgers et al., 2020). In the North Atlantic, the physical ventilation and its weakening with warming is also important and acts to further reduce the ocean carbon uptake with climate change (Yoshikawa et al., 2008; Tjiputra et al., 2010; Roy et al., 2011). In the Southern Ocean, changes in the cycling of biological material with climate change are significant and can partly counteract the reduction in the ocean carbon uptake due to the decrease in solubility and physical ventilation with warming (Sarmiento et al., 1998; Bernardello et al., 2014).

The ocean carbon cycle feedbacks can be defined on either the cumulative ocean carbon uptake or the ocean carbon storage (Schwinger et al., 2014; Arora et al., 2020). For the global ocean, these two definition are almost equivalent apart from a small contribution from the land-to-ocean carbon flux from river runoff and the carbon burial in ocean sediments (Arora et al., 2020). However, on a regional scale these two definitions are different, as the ocean carbon storage explicitly includes the transport of carbon amongst the different regions by the ocean circulation. This transport effect leads to different geographical patterns for the ocean carbon storage and the ocean cumulative carbon uptake (Frölicher et al., 2015). This transport effect also leads to a broadly similar geographical distribution for ocean carbon and heat storage, with the "redistribution" of the pre-industrial carbon and heat by changes in the circulation with warming driving a second order asymmetry between the regional patterns of heat and carbon storage (Winton et al., 2013; Bronselaer and Zanna, 2020; Williams et al., 2020). The combined air-sea transfer and transport effect leads to the Atlantic, Pacific and Southern Oceans each storing about 25-30% of the additional heat and carbon in CMIP6 models for a quadrupling of atmospheric $CO_2$ (Fig. 1a and b), despite their different size. The Atlantic Ocean has the largest increase in carbon and heat per unit volume, as given by the dissolved inorganic carbon and temperature (Fig. 1c and d). The Pacific Ocean has the smallest increase in carbon and heat per unit volume (Fig. 1c and d). Hence, our motive is to explore the mechanisms that lead to this regional variation in the carbon storage and the carbon cycle feedbacks for the different ocean basins in CMIP6 models.

A mechanism that can affect the regional carbon storage is the Atlantic Meridional Overturning Circulation (AMOC). The projected weakening in AMOC with climate change (Cheng et al., 2013) weakens the ocean physical ventilation and transport

https://doi.org/10.5194/bg-2020-487
Preprint. Discussion started: 4 January 2021


of carbon into the ocean interior, which acts to reduce the ocean carbon uptake and storage (Sarmiento and Le Quéré, 1996; Crueger et al., 2008). The weakening in AMOC with climate change also increases the residence time in the ocean interior and changes the cycling of biological material, which acts to increase the ocean carbon uptake and storage (Sarmiento and Le Quéré, 1996; Joos et al., 1999; Zickfeld et al., 2008; Bernardello et al., 2014). Previous studies suggest that the combined effect of these two competing processes leads to a modest reduction in ocean carbon uptake and storage with AMOC weakening, and an ocean carbon-climate feedback that amplifies the increase in atmospheric $CO_2$ (Sarmiento and Le Quéré, 1996; Joos et al., 1999; Crueger et al., 2008; Schwinger et al., 2014). However, the net effect of AMOC weakening with climate change on the carbon storage is highly uncertain and sensitive to the representation of the vertical carbon gradient and ocean biological processes in Earth system models. This uncertainty motivate us to explore the control of AMOC on the carbon cycle feedbacks in CMIP6 models, and the relative importance of changes in biological processes and physical ventilation for the carbon storage in different ocean basins.

Our aim is to provide insight for the relative contribution from different ocean basins to the ocean carbon cycle feedbacks, and the processes that drive this relative contribution and its uncertainty amongst CMIP6 Earth system models, with particular emphasis on the control of AMOC. In the next section, we provide a theoretical separation of the ocean carbon cycle feedbacks into contribution from carbonate chemistry, physical ventilation and biological processes, and explore how the interplay of these processes drives the global response of 10 CMIP6 Earth system models (Table 1). In section 3, we explore the geographical distribution of the ocean carbon cycle feedbacks, and the processes that control their relative distribution in the Atlantic, Pacific, Indian and Southern Oceans. In section 4, we investigate the effect of the AMOC on the global and basin-scale carbon cycle feedbacks, firstly in an idealised climate model that provides a mechanistic insight, and then in diagnostics of the CMIP6 models. Section 5 summarises our conclusions and discuss our results in the context of previous studies.

## 2 Ocean carbon cycle feedbacks and their control by different processes

Anthropogenic carbon emissions drive an increase in atmospheric $CO_2$ which in turn leads to an increase in the ocean carbon inventory relative to the pre-industrial, $\Delta I_{ocean}$. At the same time the increase in atmospheric $CO_2$ modifies the physical climate system, such as for example leading to ocean warming and increase in stratification, which further influences the ability of the ocean to absorb carbon from the atmosphere. Hence, the ocean carbon uptake due to anthropogenic carbon emissions can be expressed as a function, $F$, of changes in the atmospheric $CO_2$ and the physical climate

$$\Delta I_{ocean} = F(CO_{2,0} + \Delta CO_2, T_0 + \Delta T) - F(CO_{2,0}, T_0), \quad (1)$$

where the surface air temperature, $T$, is used as a proxy for the physical climate and subscript $_0$ is the pre-industrial. By expanding the function $F$ into a Taylor series (Schwinger et al., 2014; Williams et al., 2019), the ocean carbon inventory changes relative to the pre-industrial, $\Delta I_{ocean}$, are expressed as

https://doi.org/10.5194/bg-2020-487
Preprint. Discussion started: 4 January 2021




$$\Delta I_{ocean} = \left.\frac{\partial F}{\partial CO_2}\right|_0 \Delta CO_2 + \left.\frac{\partial F}{\partial T}\right|_0 \Delta T + \left.\frac{\partial^2 F}{\partial CO_2 \partial T}\right|_0 \Delta CO_2 \Delta T \quad (2)$$

$$+ \left.\frac{\partial^2 F}{\partial CO_2^2}\right|_0 \Delta CO_2^2 + \left.\frac{\partial^2 F}{\partial T^2}\right|_0 \Delta T^2 + R^3, \quad (3)$$

where $R^3$ contains the derivatives of third order and higher. By ignoring the second and higher order terms but keeping the terms for the non-linear relationship between atmospheric $CO_2$ and climate change, Eq. (3) is rewritten as

$$\Delta I_{ocean} = \beta_{ocean} \Delta CO_2 + \gamma_{ocean} \Delta T + \mathcal{N} \Delta CO_2 \Delta T, \quad (4)$$

where the ocean carbon-concentration feedback parameter is defined as $\beta_{ocean} = \left.\frac{\partial F}{\partial CO_2}\right|_0$, the ocean carbon-climate feedback parameter is defined as $\gamma_{ocean} = \left.\frac{\partial F}{\partial T}\right|_0$ and the non-linearity of the ocean carbon cycle feedbacks is defined as $\mathcal{N} = \left.\frac{\partial^2 F}{\partial CO_2 \partial T}\right|_0$.

The carbon cycle feedback parameters, $\beta$ and $\gamma$ , are traditionally estimated using Earth system model simulations with the couplings between the carbon cycle and radiative forcing either switched on or off: a fully coupled simulation, a radiatively coupled simulation and a biogeochemically coupled simulation (Friedlingstein et al., 2006; Arora et al., 2013; Jones et al., 2016; Arora et al., 2020). Any combination of these three simulations can be used to estimate the carbon cycle feedback parameters, however, each combination yields somewhat different results due to the non-linearity of the system (Gregory et al., 2009; Zickfeld et al., 2011; Schwinger et al., 2014; Arora et al., 2020). Here, we estimate the carbon cycle feedback parameters using the fully coupled simulation (COU) and the biogeochemically coupled simulation (BGC) under the 1% $yr^{-1}$ increasing $CO_2$ experiment, in which the atmospheric $CO_2$ concentration increases from its pre-industrial value of around 285 ppm until it quadruples over a 140-year period, following the recommended $C^4$MIP protocol of experiments (Jones et al., 2016; Arora et al., 2020). To exclude model biases, the control run was used to estimate the changes relative to the pre-industrial in the Earth system models. For simplicity, we ignore the effect of the air temperature increase in the BGC simulation to the feedbacks, which has a contribution of less than 5% (Arora et al., 2020), such that

$$\begin{aligned} \beta_{ocean} &= \frac{\Delta I^{BGC}_{ocean}}{\Delta CO_2}, \\ \gamma_{ocean} &= \frac{\Delta I^{COU}_{ocean} - \Delta I^{BGC}_{ocean}}{\Delta T}, \end{aligned} \quad (5)$$

where $\Delta CO_2$ is the increase in atmospheric $CO_2$ and $\Delta T$ the increase in air surface temperature in the fully coupled earth system (i.e COU simulation). The carbon-climate feedback parameter, $\gamma_{ocean}$, in Eq. (5) corresponds to the effect of climate change under rising atmospheric $CO_2$ and hence includes the effect of the non-linearity, $\mathcal{N} \Delta CO_2$ in Eq. (4) (Schwinger et al., 2014).

To gain insight for the driving mechanisms of the carbon cycle feedbacks and their uncertainty amongst Earth system models, $\beta_{ocean}$ and $\gamma_{ocean}$ may be separated into contribution from the regenerated, the saturated and the disequilibrium ocean carbon pools following Williams et al. (2019) and Arora et al. (2020). The ocean dissolved inorganic carbon, $DIC$, may be defined in

https://doi.org/10.5194/bg-2020-487
Preprint. Discussion started: 4 January 2021


Biogeosciences Discussions Open Access EGU

terms of these separate carbon pools (Ito and Follows, 2005; Williams and Follows, 2011; Lauderdale et al., 2013; Bernardello et al., 2014),

$$DIC = DIC_{pref} + DIC_{reg} = DIC_{sat} + DIC_{dis} + DIC_{reg}, \tag{6}$$

where $DIC_{pref}$ is the $DIC$ at the surface that is transferred into the ocean interior due to the physical ventilation, involving the circulation, and $DIC_{reg}$ is the $DIC$ accumulated into the ocean interior due to biological regeneration of organic carbon. The $DIC_{pref}$ can be further split into two idealised carbon pools: (i) the $DIC_{sat}$ representing the amount of $DIC$ that the ocean would have if the whole ocean reached a full chemical equilibrium with the contemporary atmospheric $CO_2$; and $DIC_{dis}$ representing the extend that the ocean departs from a full chemical equilibrium with the contemporary atmospheric $CO_2$. Assuming the changes in the biological organic carbon inventory are small, the changes in the ocean carbon inventory relative to the pre-industrial era may then be related to the volume integral of the changes in each of the $DIC$ pools,

$$\Delta I_{ocean} = m \int_V \left(\Delta DIC_{sat} + \Delta DIC_{dis} + \Delta DIC_{reg}\right) dV = \Delta I_{sat} + \Delta I_{dis} + \Delta I_{reg}, \tag{7}$$

where $m = 12.01 \cdot 10^{-15}$ PgC mol$^{-1}$ is a unit conversion.

By substituting Eq. (7) into Eq. (5) the ocean carbon cycle feedback parameters may be expressed in terms of these different ocean carbon pools as (Williams et al., 2019; Arora et al., 2020)

$$\begin{aligned}
\beta_{ocean} &= \beta_{sat} + \beta_{dis} + \beta_{reg} = \frac{\Delta I^{BGC}_{sat}}{\Delta CO_2} + \frac{\Delta I^{BGC}_{dis}}{\Delta CO_2} + \frac{\Delta I^{BGC}_{reg}}{\Delta CO_2}, \\
\gamma_{ocean} &= \gamma_{sat} + \gamma_{dis} + \gamma_{reg} = \frac{\Delta I^{COU}_{sat} - \Delta I^{BGC}_{sat}}{\Delta T} + \frac{\Delta I^{COU}_{dis} - \Delta I^{BGC}_{dis}}{\Delta T} + \frac{\Delta I^{COU}_{reg} - \Delta I^{BGC}_{reg}}{\Delta T}.
\end{aligned} \tag{8}$$

### 2.1 Contribution from the saturated carbon pool to $\beta_{ocean}$ and $\gamma_{ocean}$

The changes in the saturated carbon pool relative to the pre-industrial in Eq. (7) can be expressed as

$$\Delta I_{sat} = m \int_V \Delta f\left(CO_2, T_{ocean}, S, P, Si, Alk_{pre}\right) dV, \tag{9}$$

where $\Delta$ is the change relative to the pre-industrial, $T_{ocean}$ is the ocean temperature , $S$ is the ocean salinity, $P$ is the ocean phosphate concentration, $Si$ is the ocean silicate concentration, $Alk_{pre}$ is the preformed alkalinity and $f$ is a non-linear function representing the solution to the ocean carbonate chemistry for the contemporary atmospheric $CO_2$. Here, $f$ is estimated following the iterative solution for the ocean carbonate chemistry of Follows et al. (2006) and by considering the small contribution of minor species (borate, phosphate, silicate) to the preformed alkalinity. The preformed alkalinity is estimated from a multiple linear regression using salinity and the conservative tracer $PO$ (Gruber et al., 1996), with the coefficients of this regression estimated based on the upper ocean (first 10 m) alkalinity, salinity, oxygen, and phosphate in each of the Earth system models.

https://doi.org/10.5194/bg-2020-487
Preprint. Discussion started: 4 January 2021


Substituting Eq. (9) in Eq. (8) the saturated part of $\beta_{ocean}$ and $\gamma_{ocean}$ are expressed as

$$\beta_{sat} = \frac{m}{\Delta CO_2} \int_V \Delta f\left(CO_2, T_{ocean}^{BGC}, S^{BGC}, P^{BGC}, Si^{BGC}, Alk_{pre}^{BGC}\right) dV, \tag{10}$$

$$\gamma_{sat} = \frac{m}{\Delta T} \int_{V_n} \left(\Delta f\left(CO_2, T_{ocean}^{COU}, S^{COU}, Alk_{pre}^{COU}, P^{COU}, Si^{COU}\right) - \Delta f\left(CO_2, T_{ocean}^{BGC}, S^{BGC}, Alk_{pre}^{BGC}, P^{BGC}, Si^{BGC}\right)\right) dV. \tag{11}$$

To understand how the ocean carbonate chemistry operates and the mechanisms that control $\beta_{sat}$, consider an ocean buffer factor, $B$, where the fractional change in the atmospheric $CO_2$ and saturated carbon inventory is defined relative to the pre-industrial (Katavouta et al., 2018)

$$B = \frac{\Delta CO_2 / CO_{2,0}}{\Delta I_{sat} / I_{sat,0}}, \tag{12}$$

where subscript $_0$ is the pre-industrial.

Substituting Eq. (12) into Eq. (8) the saturated part of $\beta$ can be expressed as

$$\beta_{sat} = \frac{1}{B(CO_2, T_{ocean,0}, S_0, Alk_{pre,0})} \frac{I_{sat,0}}{CO_{2,0}}, \tag{13}$$

where $B(CO_2, T_{ocean,0}, S_0, Alk_0)$ is the ocean buffer factor for the contemporary atmospheric $CO_2$ under the pre-industrial ocean state for temperature, salinity and alkalinity, as is the case in the BGC run.

Expression (13) shows that $\beta_{sat}$ is proportional to the ocean capacity to buffer changes in atmospheric $CO_2$ with no changes in the physical climate, $B(CO_2, T_{ocean,0}, S_0, Alk_{pre,0})^{-1}$. The rise in atmospheric $CO_2$ leads to an increase in the saturated ocean carbon inventory, $\Delta I_{sat}$, (Fig. 2a, red shade) but also to a decrease in the ocean capacity to buffer changes in atmospheric $CO_2$ as the ocean acidifies, such that the buffer factor, $B$, increases and $\beta_{sat}$ decreases in all the Earth system models (Fig. 2b, red shade). The buffer factor, $B$, and so $\beta_{sat}$ also depend on the pre-industrial ocean state due to the non-linearity of the ocean carbonate system. Hence, there is a spread in $\beta_{sat}$ amongst the Earth system models forced by the same increase in atmospheric $CO_2$ (Fig. 2b, red shade) related to their different pre-industrial ocean temperature, salinity and alkalinity.

To understand the mechanisms that control $\gamma_{sat}$ consider the solution to the saturated part of $DIC$ as dictated by the carbonate chemistry

$$\begin{aligned} DIC_{sat} &= [CO_2]_{sat} + [HCO_3^-]_{sat} + [CO_3^{2-}]_{sat} \\ &= CO_2 \left(K_o + \frac{K_o K_1}{[H^+]_{sat}} + \frac{K_o K_1 K_2}{[H^+]_{sat}^2}\right), \end{aligned} \tag{14}$$

where

$$[CO_2]_{sat} = K_o CO_2,$$

$$[HCO_3^-]_{sat} = CO_2 K_o \frac{K_1}{[H^+]_{sat}},$$

$$[CO_3^{2-}]_{sat} = CO_2 K_o \frac{K_1 K_2}{[H^+]_{sat}^2},$$

https://doi.org/10.5194/bg-2020-487
Preprint. Discussion started: 4 January 2021


Biogeosciences Discussions Open Access EGU

and $K_o$ is the solubility, $K_1$ and $K_2$ are the ocean carbon dissociation constants, and $[H^+]_{sat}$ is the ocean hydrogen ion concentration at a chemical equilibrium with the contemporary atmospheric $CO_2$. $K_o$, $K_1$ and $K_2$ are a function of the ocean temperature and salinity and so depend on the physical climate change, while $[H^+]_{sat}$ depends primary on the changes in atmospheric $CO_2$. Combining Eq. (14) with Eq. (7) and Eq. (8), and assuming that the ocean temperature and salinity remain at their pre-industrial value in the BGC run with no climate change, $\gamma_{sat}$ can be expressed as

$$\gamma_{sat} = \frac{m}{\Delta T} \int_V CO_2 \left( \Delta K_o + \frac{\Delta (K_o K_1)}{[H^+]_{sat}} + \frac{\Delta (K_o K_1 K_2)}{[H^+]^2_{sat}} \right) dV. \tag{15}$$

By expanding $[H^+]_{sat} = [H^+]_{sat,0} + \Delta[H^+]_{sat}$, Eq. (15) can be written as

$$\gamma_{sat} = \frac{m}{\Delta T} CO_2 \int_V \Bigg( \underbrace{\left\{ \Delta K_o + \frac{\Delta (K_o K_1)}{[H^+]_{0,sat}} + \frac{\Delta (K_o K_1 K_2)}{[H^+]^2_{0,sat}} \right\}}_{\text{effect of ocean warming under } pH_0} - \underbrace{\left\{ \frac{\Delta (K_o K_1)}{[H^+]_{0,sat}} \frac{\Delta [H^+]_{sat}}{[H^+]_{sat}} + \frac{\Delta (K_o K_1 K_2)}{[H^+]^2_{0,sat}} \frac{\Delta \left( [H^+]^2_{sat} \right)}{[H^+]^2_{sat}} \right\}}_{\text{effect of ocean warming under } \Delta pH} \Bigg) dV. \tag{16}$$

The term inside the first $\{\}$ brackets in the right hand side of Eq. (16) contributes to the linear part of $\gamma_{sat}$ and is controlled by changes in climate only; specifically by the effect of changes in the ocean temperature to the solubility and ocean carbon dissociation constants. Under warming due to changes in climate this term is negative. The term inside the second $\{\}$ brackets in the right hand side of Eq. (16) contributes to the non-linear part of $\gamma_{sat}$, and it depends on changes in pH, due to the increase in atmospheric $CO_2$, and changes in climate. Under rising atmospheric $CO_2$ and warming this term is negative as $[H^+]_{sat}$ increases and $K_o$ decreases, and is smaller than the linear term as $\frac{\Delta [H^+]_{sat}}{[H^+]_{sat}} < 1$. The adjustment of $\gamma_{sat}$ due to changes in the pH, represented by this non-linear term, depends on the increase in atmospheric $CO_2$; for example, the non-linear term is about 30% and 50% of the linear term for a doubling of atmospheric $CO_2$ and for a quadrupling of atmospheric $CO_2$, respectively. Hence, the non-linearity of the carbonate chemistry acts to reduce the magnitude of the negative $\gamma_{sat}$ consistent with the carbonate system being less sensitive to change in temperature under higher ocean $DIC$ (Schwinger et al., 2014).

Expression (16) shows that $\gamma_{sat}$ is proportional to the changes in solubility due to climate change, and is further modified by changes in the ocean carbon dissociation constants with warming and by the non-linearity of the carbonate chemistry. Ocean warming due to climate change leads to a decrease in the saturated carbon inventory, $\Delta I_{sat}$, in all the Earth system models (Fig. 2c, red shade) primary driven by a decrease in solubility. This decrease in $\Delta I_{sat}$ with warming drives a nearly constant negative $\gamma_{sat}$ (Fig. 2d, red shade) with the deviations from a constant value being associated to the non-linearity of the carbonate system. The small spread of $\gamma_{sat}$ amongst the Earth system models (Fig. 2d, red shade) is associated with different pre-industrial ocean states in the models.

https://doi.org/10.5194/bg-2020-487
Preprint. Discussion started: 4 January 2021


Biogeosciences Discussions

### 2.2 Contribution from the regenerated carbon pool to $\beta_{ocean}$ and $\gamma_{ocean}$

Assuming that the oxygen concentration is close to saturation at the surface, $DIC_{reg}$ can be calculated from the apparent oxygen utilization, $AOU$, and the contribution of biological calcification to the alkalinity, $Alk$, (Ito and Follows, 2005; Williams and Follows, 2011; Lauderdale et al., 2013), such that $\Delta I_{reg}$ in Eq. (7) is expressed as

$$\Delta I_{reg} = m \int_V \left( R_{CO} \Delta AOU + \frac{1}{2} \left( \Delta Alk - \Delta Alk_{pre} - R_{NO} \Delta AOU \right) \right) dV, \tag{17}$$

where $R_{CO}$ and $R_{NO}$ are constant stoichiometric ratios, and $Alk_{pre}$ is the preformed alkalinity such that $Alk - Alk_{pre}$ gives the contribution to alkalinity from biological calcification.

Substituting Eq. (17) in Eq. (8) the regenerated part of $\beta_{ocean}$ and $\gamma_{ocean}$ are expressed as

$$\beta_{reg} = \frac{m}{\Delta CO_2} \int_V \left( R_{CO} \Delta AOU^{BGC} + \frac{1}{2} \left( \Delta Alk^{BGC} - \Delta Alk_{pre}^{BGC} - R_{NO} \Delta AOU^{BGC} \right) \right) dV, \tag{18}$$

$$\gamma_{reg} = \frac{m}{\Delta T} \int_V \Bigg( R_{CO} \left( \Delta AOU^{COU} - \Delta AOU^{BGC} \right) + \frac{1}{2} \left( \Delta Alk^{COU} - \Delta Alk^{BGC} - \Delta Alk_{pre}^{COU} + \Delta Alk_{pre}^{BGC} - R_{NO} \left( \Delta AOU^{COU} - \Delta AOU^{BGC} \right) \right) \Bigg) dV. \tag{19}$$

The regenerated part of $\beta_{ocean}$ is associated with changes in ocean biological processes due to the atmospheric $CO_2$ increase. $\Delta I_{reg}^{BGC}$ and $\beta_{reg}$ are effectively negligible in the Earth system models (Fig. 2a and b, green shade) as these models do not include an explicit dependence of biological production to an increase in carbon availability or decrease in seawater pH. The regenerated part of $\gamma_{ocean}$ is associated with changes in ocean biological processes due to changes in climate, including the effect of changes in the circulation on the sinking rate of particles, the effect of warming on the solubility of oxygen and the effect of changes in alkalinity on the dissolution of the calcium carbonate shells of calcifying phytoplankton. $\Delta I_{reg}^{COU} - \Delta I_{reg}^{BGC}$ and $\gamma_{reg}$ are positive and increase in time in all the Earth system models (Fig. 2c and d, green shade), as $\gamma_{reg}$ is dominated by the weakening in the ocean physical ventilation due to climate change. This weakening in the ocean physical ventilation leads to a longer residence time of water masses in the ocean interior and so to an increase in the accumulation of carbon from the regeneration of biologically cycled carbon in the deep ocean (Schwinger et al., 2014; Bernardello et al., 2014).

### 2.3 Contribution from the disequilibrium carbon pool to $\beta_{ocean}$ and $\gamma_{ocean}$

The disequilibrium part of $\beta_{ocean}$ and $\gamma_{ocean}$ are estimated using Eq. (8) as

$$\beta_{dis} = \beta_{ocean} - \beta_{sat} - \beta_{reg} = \frac{\Delta I_{ocean}^{BGC}}{\Delta CO_2} - \frac{\Delta I_{sat}^{BGC}}{\Delta CO_2} - \frac{\Delta I_{reg}^{BGC}}{\Delta CO_2}, \tag{20}$$

https://doi.org/10.5194/bg-2020-487
Preprint. Discussion started: 4 January 2021


Biogeosciences Discussions Open Access EGU

and

$$\gamma_{dis} = \gamma_{ocean} - \gamma_{sat} - \gamma_{reg} = \frac{\Delta I^{COU}_{ocean} - \Delta I^{BGC}_{ocean}}{\Delta T} - \frac{\Delta I^{COU}_{sat} - \Delta I^{BGC}_{sat}}{\Delta T} - \frac{\Delta I^{COU}_{reg} - \Delta I^{BGC}_{reg}}{\Delta T}. \quad (21)$$

The disequilibrium part of the carbon cycle feedback parameters is controlled by the ocean physical ventilation. Specifically, $\beta_{dis}$ is a function of the pre-industrial ocean physical ventilation and the rate of transfer of the anthropogenic carbon from the ocean surface into the ocean interior. The rise in atmospheric $CO_2$ leads to an increase in the magnitude of the negative disequilibrium ocean carbon inventory, $\Delta I_{dis}$, in all the Earth system models (Fig. 2a, blue shade), as the ocean physical ventilation is relatively slow and the ocean carbon transfer over the ocean interior cannot keep up with the rate of increase in atmospheric $CO_2$. Hence, $\beta_{dis}$ is negative in all the Earth system models (Fig. 2b, blue shade). However, the rate of increase in the negative $\Delta I_{dis}$ slows down in time (Fig. 2a, blue shade) and $\beta_{dis}$ becomes less negative in time (Fig. 2b, blue shade), as more anthropogenic carbon is transferred into the ocean interior while the buffer capacity of the ocean decreases, which brings the ocean closer to an equilibrium with the contemporary atmospheric $CO_2$.

The disequilibrium part of $\gamma_{ocean}$ depends on the weakening of the ocean physical ventilation with climate change. Here, $\gamma_{dis}$ is defined based on the climate change impact under rising atmospheric $CO_2$ (i.e., COU-BGC runs) and so includes: (i) the effect of the ventilation weakening on the pre-industrial ocean carbon gradient involving the natural carbon; and (ii) the effect of the ventilation weakening on the anthopogenic carbon. Overall, the effect of the ventilation weakening on the combined anthopogenic and natural carbon leads to a negative $\Delta I_{dis}$ and a negative $\gamma_{dis}$ on a global scale after year 40 (Fig. 2c and d, blue shade). The disequilibrium part of $\gamma_{ocean}$ becomes more negative in time in all the Earth system models as the ocean ventilation becomes weaker with warming.

### 2.4 Combined effect of saturated, disequilibrium and regenerated carbon pools to $\beta_{ocean}$ and $\gamma_{ocean}$

On a global scale, the ocean carbon-concentration feedback parameter, $\beta_{ocean}$, is positive in all the Earth system models and explained by the chemical response involving the rise in ocean saturation, $\beta_{sat}$, opposed by the effect of the relatively slow ocean ventilation, such that the physical uptake of carbon within the ocean is unable to keep pace with the rise in atmospheric $CO_2$, $\beta_{dis}$ (Fig. 2b). There is no significant contribution from biological changes to $\beta_{ocean}$ in the Earth system models (Fig. 2b, green shading). The spread in $\beta_{ocean}$ amongst the Earth system models is relatively small (coefficient of variation, CV, of 0.10) when compared with the spread in $\gamma_{ocean}$ (CV of 0.46) (Table 2). The spread in $\beta_{sat}$ is small (Fig. 2b, red shading) reflecting the use of similar carbonate chemistry schemes and bulk parameterizations of air–sea $CO_2$ fluxes across marine biogeochemical models in CMIP6 (Séférian et al., 2020), and is driven from differences in the pre-industrial ocean state, involving ocean temperature, salinity and alkalinity, amongst the models due to the non-linearity of ocean carbonate chemistry. The spread in $\beta_{dis}$ is also small (Fig. 2b, blue shading) as all the Earth system models have a broadly similar general pre-industrial circulation and physical ventilation.

The ocean carbon-climate feedback parameter, $\gamma_{ocean}$, is negative in the Earth system models, suggesting that the ocean takes up less carbon in response to climate change. The decrease in solubility and in the physical ventilation with warming act to reduce the ocean carbon uptake leading to a negative $\gamma_{sat}$ and $\gamma_{dis}$, respectively (Fig. 2d). However, the decrease in

https://doi.org/10.5194/bg-2020-487
Preprint. Discussion started: 4 January 2021


the physical ventilation with warming also acts to increase the residence time in the ocean interior leading to an increase in the regenerated carbon and a positive $\gamma_{reg}$ (Fig. 2d, green shading). The combined $\gamma_{sat}$ and $\gamma_{dis}$ dominate over the opposing $\gamma_{reg}$ leading to an overall negative $\gamma_{ocean}$. The model spread in $\gamma_{ocean}$ is mainly driven by the spread in $\gamma_{dis}$ and $\gamma_{reg}$ (Fig. 2d) and it is associated with the different response of the ocean ventilation to warming in these models. The spread in $\gamma_{reg}$ is larger than the spread in $\gamma_{dis}$ due to the different parametrizations of ocean biogeochemical processes in the models. The spread in $\gamma_{sat}$ is relatively small (Fig. 2d, red shading) as all the models use similar carbonate chemistry schemes, and is driven by the non-linearity of the carbonate system that leads to a small sensitivity of $\gamma_{sat}$ to the spread in the pre-industrial ocean temperature, salinity and alkalinity.

## 3 Regional ocean carbon cycle feedbacks in CMIP6 Earth system models

The carbon cycle feedbacks for the global ocean in Eq. (4) can be further separated into contribution from different ocean regions such that

$$\sum_{n=1}^{global} \Delta I_n = \sum_{n=1}^{global} \beta_n \Delta CO_2 + \sum_{n=1}^{global} \gamma_n \Delta T, \tag{22}$$

where $\gamma_n$ includes the non-linearity of the ocean carbon cycle feedbacks, $n$ notes the different ocean regions, $\Delta I_n$ is the change in the ocean carbon inventory relative to the pre-industrial in the region $n$, $\Delta CO_2$ and $\Delta T$ are the global changes in atmospheric $CO_2$ and the surface air temperature, respectively, and $\beta_n$ and $\gamma_n$ are the carbon cycle feedback parameters for each ocean region $n$ expressed as

$$\begin{aligned} \beta_n &= \frac{\Delta I_n^{BGC}}{\Delta CO_2}, \\ \gamma_n &= \frac{\Delta I_n^{COU} - \Delta I_n^{BGC}}{\Delta T}. \end{aligned} \tag{23}$$

In Eq. (23) the regional feedback parameters are defined by the regional ocean carbon storage rather than the regional cumulative ocean carbon uptake, so that they include the effects from local air-sea carbon exchange and from the ocean transport of carbon between the different regions.

This effect of the ocean transport on carbon storage is important and when accounted for leads to different spatial patterns for the carbon cycle feedback parameters (Fig. 3). Specifically, the carbon-concentration feedback parameter, $\beta$, estimated from the regional cumulative ocean $CO_2$ uptake (Fig. 3b) is large in the Southern Ocean, the North Atlantic, the Kuroshio Extension and the eastern boundary upwelling regions, and small in the subtropical gyres. The carbon-concentration feedback parameter, $\beta$, estimated from the regional ocean carbon storage (Fig. 3a) is also large in the North Atlantic, but instead large in the South hemisphere subtropical gyres and small in the Southern Ocean south of 50$^o$S. This difference in the $\beta$ estimated from the cumulative ocean $CO_2$ uptake and the ocean carbon storage is due to the northward transport of anthropogenic carbon from the Southern Ocean associated with subduction and transport of mode and intermediate waters.

The carbon-climate feedback parameter, $\gamma$, estimated from the regional cumulative ocean $CO_2$ uptake due to climate change (Fig. 3b) is large and negative in the North Atlantic and in the Southern Ocean between 50$^o$S to 65$^o$S, and large and positive

https://doi.org/10.5194/bg-2020-487
Preprint. Discussion started: 4 January 2021


Biogeosciences Discussions Open Access EGU

in a narrow band between 40$^o$S to 45$^o$S, in the South hemisphere eastern boundary upwelling regions and in areas with sea ice like the Arctic and around Antarctic. The transport effect redistributes spatial asymmetries in $\gamma$, driven by the regional air-sea carbon exchange, and leads to a more uniform and less negative $\gamma$ in the Southern Ocean, a less negative $\gamma$ in the North Atlantic high latitudes and a switch to a negative $\gamma$ in the Arctic (Fig. 3.a). For diagnostics of the net effect of the ocean transport on the carbon storage and the carbon cycle feedbacks in the Atlantic, Pacific and Southern Oceans see the Appendix.

Here, we focus on the ocean carbon cycle feedbacks estimated from the regional ocean carbon storage to gain more mechanistic insight, so as (i) to account explicitly for the ocean transport of carbon, and (ii) to enable estimates of the regional contribution from the changes in the saturated, disequilibrium and regenerated carbon pools.

### 3.1 Contribution from different basins to $\beta_{ocean}$ and $\gamma_{ocean}$

The Atlantic, Pacific and Southern Oceans contribute equally to the ocean carbon-concentration feedback parameter, $\beta_{ocean}$, (Fig. 4a) with an inter-model mean of 0.22, 0.25 and 0.23 PgC ppm$^{-1}$, respectively (Table 2). The Indian Ocean contributes less than half than the other 3 basins to $\beta_{ocean}$ (Fig. 4a) with an inter-model mean of 0.10 PgC ppm$^{-1}$ (Table 2). In contrast, the contribution to the saturated and disequilibrium carbon pools, $\beta_{sat}$ and $\beta_{dis}$, follows the basin size, with the Pacific Ocean having the largest contribution and the Indian Ocean the smallest contribution (Fig. 4a). In all basins, $\beta_{reg}$ is more than an order of magnitude smaller than $\beta$ (Fig. 4a). There is a relative small spread in $\beta$, as shown by the coefficient of variation, CV<0.13 in all basins, (Table 2), and in $\beta_{sat}$ and $\beta_{dis}$ amongst the Earth system models (Fig. 4a).

The Pacific, Atlantic, Southern and Indian Oceans contribution to the ocean carbon-climate feedback parameter, $\gamma_{ocean}$, is on average -5.0, -4.5, -3.1 and -1.2 PgC K$^{-1}$, respectively (Table 2 and Fig. 4b). The basin-wide variability in $\gamma$ amongst the models, as described by the coefficient of variation, CV, varies from 0.56 in the Pacific Ocean to 0.92 in the Southern Ocean (Table 2). The variability in $\gamma$ amongst the models for each basin is substantially larger than that of the global ocean (Table 2), which suggests that variability in different basins can compensate each other.

In the Southern Ocean, the contribution of the saturated, disequilibrium and regenerated carbon pools to $\gamma$ is of a similar magnitude (Fig. 4b, blue circles), such that the decrease in solubility, the reduction in the physical ventilation and the increase in the regenerated carbon accumulation in the ocean interior due to climate change are equally important. In the Atlantic Ocean, $\gamma$ is dominated by the disequilibrium carbon pool (Fig. 4b, red circles) and the reduction in the physical ventilation due to climate change, with the contribution of the regenerated and the saturated carbon pools being of a smaller magnitude. In the Indian Ocean, $\gamma$ is mainly controlled by the compensation between saturated and regenerated carbon pools (Fig. 4b, yellow circles). In the Pacific Ocean, the magnitude of $\gamma$ is dominated by the saturated carbon pool and the decrease in carbon solubility due to warming (Fig. 4b, purple circles). In all basins, the spread in $\gamma_{dis}$ and $\gamma_{reg}$ amongst the models is relative larger compare to the spread in $\gamma_{sat}$ (Fig. 4b). Hence, in all the ocean basins, the spread in $\gamma$ amongst the models is mainly driven by the inter-model variability in the response of the physical ventilation and the regenerated carbon to climate change.

https://doi.org/10.5194/bg-2020-487
Preprint. Discussion started: 4 January 2021


Biogeosciences Discussions Open Access EGU

### 3.2 Processes controlling the contribution from different basins to $\beta_{ocean}$ and $\gamma_{ocean}$

The discrepancy between the basins volume relative to the global ocean, and the basins fractional contribution to $\beta_{ocean}$ and $\gamma_{ocean}$ (Fig. 5) suggests that larger regions do not necessary store more carbon, but rather the ocean carbon cycle feedbacks depend upon a complex interplay between ocean transport, air-sea interaction and biological processes.

The Southern and Indian Oceans contribute 27% and 12%, respectively, to the ocean carbon-concentration feedback parameter, $\beta_{ocean}$, following their fractional volumes of the global ocean (Fig. 5a). The Atlantic Ocean contributes 26% to $\beta_{ocean}$, significantly more than its fractional volume of 18% of the global ocean. In contrast, the Pacific ocean contributes only 30% to $\beta_{ocean}$ despite its fractional volume of 42% of the global ocean. By definition, the contribution of each basin to $\beta_{sat}$ and $\beta_{dis}$ is approximately proportional to the ocean volume contained in each basin. However, $\beta_{dis}$ is relatively low in the Atlantic Ocean and high in the Pacific Ocean compared with their respective volumes, which is consistent with the Atlantic Ocean interior being more ventilated and closer to equilibrium with the contemporary atmospheric $CO_2$, and the Pacific ocean interior being less ventilated than the rest of the ocean. Hence, the relative large contribution to $\beta_{ocean}$ from the Atlantic Ocean is associated with a strong and rapid transfer of anthropogenic carbon into the ocean interior from both a strong local physical ventilation and a transport of carbon from the Southern Ocean.

The Atlantic Ocean has a contribution of 30% to $\gamma_{ocean}$, much larger than expected from its fractional volume of 18% of the global ocean (Fig. 5b). This large contribution of the Atlantic Ocean is primarily due to the disequilibrium part of $\gamma$ (Fig. 5b), and the reduction in the physical ventilation due to climate change. In the well ventilated Atlantic Ocean, the additional heat penetrates into the ocean interior and is not confined to the ocean surface, which limits the effect of the reduction in solubility with warming, so that there is only a 11% contribution to $\gamma_{sat}$ there.

The Pacific and Indian Ocean contributions to $\gamma_{sat}$ are consistent with their fractional volumes (Fig. 5b). These basins experience a significant decrease in solubility despite having warmed less per unit volume than the rest of the ocean (Fig. 1d), as much of this warming is confined in the ocean mixed layer. The Pacific and Indian Ocean contributions to $\gamma_{dis}$ and $\gamma_{reg}$ are smaller than expected from their fractional volumes, as there is no significant effect from changes in ventilation. This absence of any significant effect from changes in the ventilation with warming in the Pacific and the Indian Oceans leads to their smaller contribution to $\gamma_{ocean}$ relative to their volumes (Fig. 5b).

The Southern Ocean has a contribution of 38% to $\gamma_{dis}$, and of 52% to $\gamma_{reg}$, much larger than expected from its fractional volume (Fig. 5b), which suggests that changes in the physical ventilation and the accumulation of regenerated carbon due to climate change drive large changes in ocean storage. The Southern Ocean contribution to $\gamma_{sat}$ is also larger than expected from its fractional volume (Fig. 5b), consistent with a large warming per unit volume in this basin (Fig. 1d). Hence, the apparent small contribution of the Southern Ocean to $\gamma_{ocean}$, of 20%, is due to a compensation between the large decrease in ocean carbon storage associated with the combined decrease in solubility and physical ventilation, and the large increase in ocean carbon storage associated with longer residence time and accumulation of regenerated carbon in the ocean interior there.

https://doi.org/10.5194/bg-2020-487
Preprint. Discussion started: 4 January 2021


Biogeosciences Discussions Open Access EGU

## 4 Control of the Atlantic Meridional Overturning Circulation to the carbon cycle feedbacks

The ocean carbon cycle feedbacks are controlled by the ocean ventilation and the transfer of carbon from the mixed layer to the thermocline and deep ocean. The ocean ventilation involves the seasonal cycle of the mixed layer, the subduction process and the effects of the eddy, gyre and overturning circulations. Despite this complexity the strength of the Atlantic Meridional Overturning Circulation (AMOC) and its weakening due to climate change is often used as a proxy for the large scale ocean ventilation. Here we investigate the dependence of the carbon cycle feedbacks to the AMOC strength and its weakening with climate change on the global and basin-length scales.

### 4.1 Insight from an idealised climate model with a meridional overturning

The idealised climate model of Katavouta et al. (2019) is now used to investigate the control of the AMOC to the carbon cycle feedbacks. This idealised model consists of a slab atmosphere, two upper ocean boxes for the southern and northern high latitudes, two boxes for the mixed layer and the thermocline in the low and mid latitudes, and one box for the deep ocean (Fig. 6a). The model solves for the thermocline thickness from a volumetric balance between the surface cooling conversion of light to dense waters in the North Atlantic, the diapycnic transfer of dense to light waters in low and mid latitudes, and the conversion of dense to light waters in the Southern Ocean involving an Ekman transport partially compensated by a polewards mesoscale eddy transport (Gnanadesikan, 1999; Johnson et al., 2007; Marshall and Zanna, 2014). The model also accounts for the rate of subduction occurring in the Southern Ocean versus the tropics and subtropics through an isolation fraction for water remaining below the mixed layer and spreading northwards in the thermocline. The model solves for the ocean carbon cycle including physical and chemical transfers, but ignores biological transfers, and sediment and weathering interactions involving changes in the cycling of organic carbon or calcium carbonate. The ocean carbonate system is solved using the iterative algorithm of Follows et al. (2006). For the model closures and an explicit description of the model budgets and equations see Katavouta et al. (2019).

The model is first integrated to a pre-industrial steady state, with the distribution of temperature and $DIC$ depending on the pre-industrial strength of the overturning. The model is then forced by a 1% yr$^{-1}$ increase in atmospheric $CO_2$ concentration from a pre-industrial value of 280 ppm until atmospheric $CO_2$ quadruples over a 140-year period. This increase in atmospheric $CO_2$ drives a radiative forcing: $R = a \ln(CO_2/CO_{2,0})$, where a = 5.35 W m$^{-2}$ (Myhre et al., 1998) and subscript $_0$ is the pre-industrial. This radiative forcing then drives a radiative response, $\lambda \Delta T_{air}$, and a net downward heat flux entering the system at the top of the atmosphere, $N_{TOA}$, (Gregory et al., 2004) such that $R = \lambda \Delta T_{air} + N_{TOA}$, where $T_{air}$ is the temperature of the slab atmosphere and $\lambda$ is the climate feedback parameter that is assumed constant and equal to 1 W m$^{-2}$K$^{-1}$ for simplicity. The ocean heat uptake, $N$, is distributed equally over the ocean surface and estimated as $N = N_{TOA} - c(\Delta T_{surf} - \Delta T_{air})$, where $c$=50 W m$^{-2}$ K$^{-1}$ is an air–sea heat transfer parameter and $T_{surf}$ is the ocean temperature at the surface. For this model closure, the ocean heat uptake is more than 95% of the net downward heat flux entering the system at the top of the atmosphere.

https://doi.org/10.5194/bg-2020-487
Preprint. Discussion started: 4 January 2021


This additional ocean heat reduces the conversion of light to dense waters in the North Atlantic, $q_{NA}$, and leads to an overturning weakening, following

$$\Delta q_{NA} = -\frac{AN}{\rho C_p T_{contrast}}, \tag{24}$$

where $A$ is the model area covered by the low and mid latitudes, $\rho$ is a referenced ocean density, $C_p$ is the specific heat capacity for the ocean, and $T_{contrast}$ is the temperature contrast between light waters in the low and mid latitudes, involving the mixed layer and thermocline, and the dense waters in the deep ocean.

Three experiments were conducted using this idealised model forced by 1% $yr^{-1}$ increase in atmospheric $CO_2$: (i) a control experiment with a strong pre-industrial AMOC that experiences a reduction with warming as described by Eq. (24) (solid line in Fig. 6b); (ii) an experiment with a weak pre-industrial AMOC that experiences the same reduction with warming as in the control experiment (dotted line in Fig. 6b); and (iii) an experiment with a strong pre-industrial AMOC that experiences a doubled reduction with warming than in the control experiment, such that the right hand of Eq. (24) is multiplied by a factor of 2 (dashed line in Fig. 6b). In all the experiments, a fully coupled simulation (COU) and a biogeochemically coupled simulation (BGC) are used to estimate the carbon-cycle feedback parameters $\beta_{ocean}$ and $\gamma_{ocean}$.

In the idealised model, a weaker pre-industrial meridional overturning leads to a smaller carbon-concentration feedback parameter, $\beta_{ocean}$, during the centennial transient response to the increase in atmospheric $CO_2$ (Fig. 6c, black lines). The saturated part of $\beta$ does not directly depend on the AMOC strength (Fig. 6c, red lines). In contrast, a weaker pre-industrial AMOC leads to a more negative disequilibrium part of $\beta$ (Fig. 6c, blue lines) due to a weaker and slower transfer of anthropogenic carbon below the ocean surface. Hence, the pre-industrial AMOC controls $\beta_{ocean}$ through its effect on the physical ventilation via the disequilibrium carbon pool.

The strength of the pre-industrial meridional overturning has only a small impact on the carbon-climate feedback parameter, $\gamma_{ocean}$, that is associated with the saturated carbon pool (Fig. 6d, solid and dotted lines). In the idealised model, a different pre-industrial overturning is associated with a different pre-industrial ocean state, in terms of temperature and $DIC$, which has a small effect in the the saturated part of $\gamma$ due to the non-linearity of the carbonate chemistry. The carbon-climate feedback parameter, $\gamma_{ocean}$, is primarily controlled by the changes in AMOC with warming, and specifically by the dependence of the negative $\gamma_{dis}$ to the AMOC reduction with warming (Fig. 6d, solid and dashed lines). Hence, a more pronounced reduction in AMOC with warming drives a more negative $\gamma_{ocean}$, as it leads to a larger reduction in the physical transfer of carbon into the ocean interior.

### 4.2 Results from CMIP6 Earth system models

There is a large spread in the pre-industrial strength of AMOC amongst the Earth system models (Fig. 7) with a range of 11.3 Sv in IPSL-CM6A-LR to 23.2 Sv in NorESM2-LM (Table 3). There is also a large spread in the response of the AMOC to climate change amongst the models (Fig. 8), with the magnitude of the AMOC weakening ranging from -3.6 Sv in IPSL-CM6A-LR to -17.47 Sv in MRI-ESM2 (Table 3). Generally, the models with a stronger pre-industrial AMOC simulate a larger

https://doi.org/10.5194/bg-2020-487
Preprint. Discussion started: 4 January 2021


reduction in AMOC with warming. Linear correlations are used to relate the AMOC variability amongst the models with the variability in the carbon-cycle feedbacks for the global ocean and the different ocean basins (Table 4).

For the global ocean, there is a moderate positive correlation between the pre-industrial AMOC and the ocean carbon-concentration feedback parameter, $\beta_{ocean}$, ($r$=0.70, Table 4), such that models with stronger pre-industrial AMOC have a more positive $\beta_{ocean}$. However, there is no significant correlation between the pre-industrial AMOC and the saturated or disequilibrium part of $\beta$ (Table 4) on global scale. In the Atlantic Ocean, $\beta$ is strongly correlated with the pre-industrial AMOC in the Earth system models ($r$=0.87) and this correlation is due to $\beta_{dis}$ (Table 4 and Fig. 9a and c), which suggests that a stronger pre-industrial AMOC leads to a larger $\beta$ via a stronger physical transfer of anthopogenic carbon below the ocean surface there, similar to the behaviour of the idealised model (Fig. 6c).

In the Southern Ocean, there is a statistically significant correlation between the pre-industrial AMOC and $\beta$ ($r$=0.82), that is not associated with either the saturated, the disequilibrium or the regenerated carbon pools (Table 4). A stronger pre-industrial AMOC is associated with a stronger return flow of interior water into the surface in the Southern Ocean upwelling branch of the overturning circulation (Marshall and Speer, 2012), and hence with a stronger local anthropogenic carbon uptake from the atmosphere in the BGC run there. However, in the Southern Ocean both the anthopogenic carbon uptake from the atmosphere and its export to the other basins are also controlled by subduction (Sabine et al., 2004; Sallée et al., 2012, 2013) and the residual circulation involving the wind-driven Ekman transport and eddy fluxes (Lauderdale et al., 2013). Hence, there is no significant correlation between the pre-industrial AMOC and $\beta_{dis}$ in the Southern Ocean as other processes like subduction and the residual circulation are important in setting the pre-industrial physical ventilation and transport of carbon to other basins. There is also no significant correlation between the pre-industrial AMOC and $\beta$ in the Pacific and Indian Oceans, suggesting that other processes dominate the ocean ventilation there.

For the global ocean, the carbon-climate feedback parameter, $\gamma_{ocean}$, and its disequilibrium part, $\gamma_{dis}$, are positively correlated with the AMOC weakening due to climate change in the Earth system models ($r$=0.67, and $r$=0.76, respectively, Table 4). This correlation for the global ocean is driven by the Atlantic Ocean, as there is no significant correlation between $\gamma$ and AMOC weakening in the Pacific, Indian and Southern Oceans (Table 4). In the Atlantic Ocean, a more pronounced AMOC weakening due to climate change is associated with a larger reduction in the physical transfer of carbon below the ocean surface and so with a more negative $\gamma$ and $\gamma_{dis}$ (Fig. 10a and c), consistent with the inferences for the idealised model (Fig. 6d)..

In the Atlantic Ocean, the correlation between $\gamma_{reg}$ and AMOC weakening is negative ($r$=-0.67, Table 4), when excluding the CNRM-ESM2-1 model which has a much larger $\gamma_{reg}$ than the rest of the Earth system models (Table 3). A more pronounced AMOC weakening leads to a longer residence time in the Atlantic Ocean interior and so to a larger accumulation of regenerated carbon there and a more positive $\gamma_{reg}$ (Fig. 10d). The substantially larger change in the regenerated carbon pool with warming in CNRM-ESM2-1 than the rest of the models is probably due to a revised parametirization for organic mater remineralization (in PISCESv2-gas), its parametrisation of sedimentation and its interactive riverine input; see Séférian et al. (2020) for differences in ocean biogeochemistry amongst the Earth system models.

https://doi.org/10.5194/bg-2020-487
Preprint. Discussion started: 4 January 2021


## 5 Discussion and Summary

Our study reveals the control of the carbonate chemistry, physical ventilation and biological processes on the relative contribution of the Atlantic, Pacific, Indian and Southern Oceans to the ocean carbon cycle feedbacks in a set of CMIP6 Earth system models. Experiments using an idealised climate model and diagnostics of the CMIP6 models suggest a dependence of the ocean carbon cycle feedbacks on the strength of the pre-industrial Atlantic Meridional Overturning Circulation (AMOC) and on the magnitudes of the AMOC weakening with warming, primarily due to the control of the AMOC on the physical ventilation in the Atlantic Ocean. .

The ocean carbon-concentration feedback in CMIP6 models is controlled by a competition between opposing contributions from the saturated and the disequilibrium carbon pools, such that (i) the carbonate chemistry drives a positive $\beta_{ocean}$ that decreases with the increase in atmospheric $CO_2$ as the ocean acidifies and its capacity to buffer atmospheric $CO_2$ decreases, and (ii) the physical ventilation drives a negative $\beta_{ocean}$ that becomes less negative in time as the anthropogenic carbon is transferred from the ocean surface into the ocean interior. The ocean carbon-climate feedback in CMIP6 models is controlled by a competition between the combined decrease in the saturated and disequilibrium carbon pools and the increase in the regenerated carbon pool, such that (i) the decrease in solubility and weakening in physical ventilation with warming drive a negative $\gamma_{ocean}$, and (ii) the increase in the accumulation of regenerated carbon, associated with a longer residence time in the ocean interior with climate change, drives a positive $\gamma_{ocean}$.

### 5.1 Regional ocean carbon cycle feedbacks

The regional ocean carbon storage is controlled by the local air-sea carbon exchange and the transport of carbon by the ocean circulation. Here, we estimated the regional carbon cycle feedbacks based on the regional ocean carbon storage such that the effect of the ocean transport of carbon is explicitly accounted for. This transport effect acts to decrease the carbon-concentration feedback parameter, $\beta$, in the Southern Ocean, and increase $\beta$ in the Southern hemisphere subtropical gyres and the western boundary of the Atlantic Ocean in CMIP6 models. The transport effect on $\beta$ is consistent with the view that while almost half of the anthopogenic carbon enters through the Southern Ocean, much of this carbon is transferred and stored into the Atlantic, Pacific and Indian Oceans (Sabine et al., 2004; Khatiwala et al., 2009; Frölicher et al., 2015). The transport effect also leads to a more spatially uniform and negative carbon-climate feedback parameter, $\gamma$, almost everywhere in the ocean in CMIP6 models.

The Atlantic, Pacific and the Southern Oceans provide comparable contributions, of 26% to 30%, to the global ocean carbon-concentration feedback, despite their different size. This large contribution from the Atlantic Ocean relative to its volume is associated with an enhanced physical transfer of anthropogenic carbon into the ocean interior due to a strong local ventilation and a transport of carbon from the Southern Ocean. The inter-model variability in the carbon-concentration feedback parameter, $\beta$, amongst the CMIP6 models is small in all the ocean basins, reflecting the use of a similar carbonate chemistry scheme in these models (Séférian et al., 2020) and a similar general large-scale circulation.

https://doi.org/10.5194/bg-2020-487
Preprint. Discussion started: 4 January 2021


The Atlantic Ocean has the largest contribution to the ocean carbon-climate feedback relative to its size in CMIP6 models, which is mainly due to the disequilibrium carbon pool and the reduction in the physical ventilation with climate change. Specifically, the negative $\gamma$ per unit area is largest in the high latitudes of the North Atlantic in CMIP6 models, consistent with previous studies suggesting the effect of climate-driven changes in the circulation to the carbon storage is significant there (Sarmiento et al., 1998; Winton et al., 2013; Bernardello et al., 2014).

The relative small contribution from the Southern Ocean to the carbon-climate feedback in CMIP6 is due to a partial compensation between the combined decrease in solubility and physical ventilation with warming, driving a negative $\gamma$, and the large increase in accumulation of regenerated carbon in the ocean interior with climate change, driving a positive $\gamma$. This compensation between the decrease in solubility and physical ventilation with warming and the increase in accumulation of regenerated carbon with climate change in the Southern Ocean is also supported by previous studies based on experiments using a single model (Sarmiento et al., 1998; Bernardello et al., 2014); and a significant increase in the regenerated carbon pool of the Southern Ocean with climate change was also found in CMIP5 models (Ito et al., 2015).

In the Indo-Pacific Ocean, the carbon-climate feedback in CMIP6 is primarily attributed to the saturated carbon pool and the decrease in solubility with warming. This response in the Indo-Pacific Ocean is consistent with a feedback triggered by warming and the reduction in solubility dominating in low and mid-latitudes, as was shown in a CMIP5-generation Earth system model (Rodgers et al., 2020). The inter-model variability in $\gamma$ amongst CMIP6 models is relatively large compared with $\beta$ in all the ocean basins, and is mainly driven by the spread in the response of physical ventilation and circulation to climate change, and in the parametrization of ocean biogeochemical processes amongst the models.

### 5.2 Control of the Altantic Meridional Overturning Circulation

Our sensitivity experiments with an idealised climate model show that a weaker pre-industrial Atlantic Meridional Overturning Circulation (AMOC) leads to a smaller ocean carbon-concentration feedback parameter, $\beta_{ocean}$. This dependence of $\beta_{ocean}$ to the pre-industrial AMOC is controlled by the disequilibrium carbon pool, and the physical transfer of anthropogenic carbon from the surface to the ocean interior. The ocean carbon-climate feedback parameter, $\gamma_{ocean}$, is instead primarily controlled by the reduction in AMOC with warming, where a weakening in AMOC reduces the physical ventilation and leads to the disequilibrium part of $\gamma$ becoming more negative.

Turning to the CMIP6 models, in the Atlantic Ocean, the carbon-concentration feedback parameter, $\beta$, is controlled by the strength of the pre-industrial AMOC, similarly to the behaviour in the idealised climate model. This control of AMOC on $\beta$ is associated with the disequilibrium carbon pool and the effect of physical ventilation, such that Earth system models with stronger AMOC have a more efficient transport of anthopogenic carbon into the ocean interior in the Atlantic Ocean. However, there is only a moderate correlation between AMOC strength and $\beta_{ocean}$ on a global scale, which suggests that other processes related to ocean ventilation, involving the wind-driven gyre circulation, mode water formation and subduction and the Southern Ocean residual circulation, are also important for regulating the ocean carbon-concentration feedback. In contrast with our results based on the idealised model and the CMIP6 models, Roy et al. (2011) found no direct dependence of $\beta_{ocean}$ to the AMOC strength in older generation Earth system models, which suggests that either: (i) the sample of 4 models used in

https://doi.org/10.5194/bg-2020-487
Preprint. Discussion started: 4 January 2021


Biogeosciences Discussions Open Access EGU

Roy et al. (2011) is too small to reveal the link between AMOC and $\beta_{ocean}$; or (ii) the dependence of $\beta_{ocean}$ to AMOC strength is more pronounced when considering estimates at the quadrupling of atmospheric $CO_2$ rather than estimates from years 2010 to 2100 in a high-emission scenario as in Roy et al. (2011).

In the Atlantic Ocean, the carbon-climate feedback parameter, $\gamma$, is controlled by the AMOC weakening with climate change in the CMIP6 models, similarly to the behaviour in the idealised climate model. This control of the AMOC weakening on $\gamma$ is: (i) primarily due to the disequilibrium carbon pool, with a more pronounced AMOC weakening driving a larger reduction in the physical transfer of carbon into the ocean interior and a more negative $\gamma$; and (ii) to a lesser extend due to the regenerated carbon pool, with a more pronounced AMOC weakening driving a larger accumulation of regenerated carbon in the ocean interior and a more positive $\gamma$. The dependence of the carbon-climate feedback to the AMOC weakening in the Atlantic Ocean is consistent with previous studies based on experiments using a single older generation Earth system model (Crueger et al., 2008; Yoshikawa et al., 2008).

On global scale, we found only a moderate dependence of $\gamma_{ocean}$ to AMOC weakening with climate change that is attributed to the Atlantic Ocean, as there is no significant correlation between $\gamma$ and AMOC weakening in the Pacific, Indian and Southern Oceans. Hence, the weakening in the AMOC due to climate change has only a modest impact on ocean carbon uptake on the global and centennial scale, consistent with previous studies (Sarmiento et al., 1998; Joos et al., 1999; Zickfeld et al., 2008).

Future work should focus on the control of the ocean carbon cycle feedbacks from other ventilation processes beyond the AMOC, such as the formation and subduction of mode and intermediate waters involving the seasonal mixed-layer cycle, and the horizontal and vertical circulation. Additionally, the regional ocean cumulative carbon uptake and carbon storage may be estimated in a dynamically based density space (Sallée et al., 2013; Meijers, 2014; Iudicone et al., 2016) to reveal the contribution of different water masses to $\beta$ and $\gamma$ (Roy et al., 2020, personal communication). Finally, we note that for a quadrupling of atmospheric $CO_2$ and on centennial time scale the carbon-concentration feedback is substantially larger than the carbon-climate feedback; however, this will not necessary be the case after the emissions cease and there is an ongoing carbon cycle and climate response as the system adjusts towards equilibrium.

## Appendix A: Contribution of air-sea flux and ocean transport to the carbon cycle feedbacks in different ocean basins

The Southern Ocean accounts on average for about half of the ocean anthopogenic carbon uptake (Fig. A1a red line) in CMIP6 Earth system model despite covering only 30% of the global ocean consistent with results from CMIP5 model during the historical period (Frölicher et al., 2015), as well as observational based estimates (Mikaloff-Fletcher et al., 2006). However, a large portion of the anthropogenic carbon entering through the Southern Ocean is transferred through the ocean circulation into the Atlantic, Indian and Pacific Oceans, with the Atlantic Ocean receiving most of this carbon (Fig. A1a) in CMIP6 models, consistent with observational-based estimates (Sabine et al., 2004; Khatiwala et al., 2009). Consequently, the carbon-concentration feedback parameter $\beta$ is substantially larger in the Southern Ocean, but smaller in the other ocean basins when estimated based on the local air-sea cumulative carbon flux (Fig. A1b, red lines) than when estimated based on the changes in the local ocean carbon storage (Fig. A1b, black lines). Turning to the carbon-climate feedback, the net effect of climate change

https://doi.org/10.5194/bg-2020-487
Preprint. Discussion started: 4 January 2021


is a carbon loss from the ocean to the atmosphere and a negative $\gamma$ in all basins (Fig. A1c, red lines). The ocean transport acts to reduce the negative $\gamma$ in the Atlantic, the Indian and Southern Oceans, but to increase the negative $\gamma$ in the Pacific Ocean (Fig. A1c, compare the red with the black lines).

*Acknowledgements.* The authors acknowledge the World Climate Research Programme, which, through its Working Group on Coupled Modelling, coordinated and promoted CMIP6, the climate modelling groups for producing and making available their model output, and the Earth System Grid Federation for archiving the data and providing access. This work was supported by the UK Natural Environmental Research Council grants NE/T007788/1 and NE/T010657/1.

*Data availability.* The data used here are from the CMIP6 simulations performed by the various modelling groups and available from the CMIP6 archive (https://esgf-node.llnl.gov/search/cmip6).

*Author contributions.* Anna Katavouta conducted the analysis, and led the interpretation of the results and writing of the manuscript. Richard G. Williams contributed to the design of the analysis, the interpretation of the results, and the writing of the manuscript.

*Competing interests.* The authors declare that they have no conflict of interest.

https://doi.org/10.5194/bg-2020-487
Preprint. Discussion started: 4 January 2021



## References

Arora, V. K., Boer, G. J., Friedlingstein, P., Eby, M., Jones, C. D., Christian, J. R., Bonan, G., Bopp, L., Brovkin, V., Cadule, P., Hajima, T., Ilyina, T., Lindsay, K., Tjiputra, J. F., and Wu, T.: Carbon-Concentration and Carbon-Climate Feedbacks in CMIP5 Earth System Models, Journal of Climate, 26, 5289–5314, https://doi.org/10.1175/JCLI-D-12-00494.1, 2013.

Arora, V. K., Katavouta, A., Williams, R. G., Jones, C. D., Brovkin, V., Friedlingstein, P., Schwinger, J., Bopp, L., Boucher, O., Cadule, P., Chamberlain, M. A., Christian, J. R., Delire, C., Fisher, R. A., Hajima, T., Ilyina, T., Joetzjer, E., Kawamiya, M., Koven, C. D., Krasting, J. P., Law, R. M., Lawrence, D. M., Lenton, A., Lindsay, K., Pongratz, J., Raddatz, T., Séférian, R., Tachiiri, K., Tjiputra, J. F., Wiltshire, A., Wu, T., and Ziehn, T.: Carbon-concentration and carbon-climate feedbacks in CMIP6 models and their comparison to CMIP5 models, Biogeosciences, 17, 4173–4222, https://doi.org/10.5194/bg-17-4173-2020, 2020.

Bernardello, R., Marinov, I., Palter, J. B., Sarmiento, J. L., Galbraith, E. D., and Slater, R. D.: Response of the Ocean Natural Carbon Storage to Projected Twenty-First-Century Climate Change, Journal of Climate, 27, 2033–2053, https://doi.org/10.1175/JCLI-D-13-00343.1, 2014.

Boer, G. J. and Arora, V.: Temperature and concentration feedbacks in the carbon cycle, Geophysical Research Letters, 36, https://doi.org/10.1029/2008GL036220, 2009.

Boer, G. J. and Arora, V.: Geographic Aspects of Temperature and Concentration Feedbacks in the Carbon Budget, Journal of Climate, 23, 775–784, https://doi.org/10.1175/2009JCLI3161.1, 2010.

Boucher, O., Servonnat, J., Albright, A. L., Aumont, O., Balkanski, Y., Bastrikov, V., Bekki, S., Bonnet, R., Bony, S., Bopp, L., Braconnot, P., Brockmann, P., Cadule, P., Caubel, A., Cheruy, F., Codron, F., Cozic, A., Cugnet, D., D'Andrea, F., Davini, P., de Lavergne, C., Denvil, S., Deshayes, J., Devilliers, M., Ducharne, A., Dufresne, J.-L., Dupont, E., Éthé, C., Fairhead, L., Falletti, L., Flavoni, S., Foujols, M.-A., Gardoll, S., Gastineau, G., Ghattas, J., Grandpeix, J.-Y., Guenet, B., Guez, Lionel, E., Guilyardi, E., Guimberteau, M., Hauglustaine, D., Hourdin, F., Idelkadi, A., Joussaume, S., Kageyama, M., Khodri, M., Krinner, G., Lebas, N., Levavasseur, G., Lévy, C., Li, L., Lott, F., Lurton, T., Luyssaert, S., Madec, G., Madeleine, J.-B., Maignan, F., Marchand, M., Marti, O., Mellul, L., Meurdesoif, Y., Mignot, J., Musat, I., Ottlé, C., Peylin, P., Planton, Y., Polcher, J., Rio, C., Rochetin, N., Rousset, C., Sepulchre, P., Sima, A., Swingedouw, D., Thiéblemont, R., Traore, A. K., Vancoppenolle, M., Vial, J., Vialard, J., Viovy, N., and Vuichard, N.: Presentation and Evaluation of the IPSL-CM6A-LR Climate Model, Journal of Advances in Modeling Earth Systems, 12, e2019MS002 010, https://doi.org/10.1029/2019MS002010, 2020.

Bronselaer, B. and Zanna, L.: Heat and carbon coupling reveals ocean warming due to circulation changes, Nature, 584, 227–233, https://doi.org/10.1038/s41586-020-2573-5, 2020.

Ceppi, P. and Gregory, J. M.: Relationship of tropospheric stability to climate sensitivity and Earth's observed radiation budget, Proceedings of the National Academy of Sciences, 114, 13 126–13 131, https://doi.org/10.1073/pnas.1714308114, 2017.

Cheng, W., Chiang, J. C. H., and Zhang, D.: Atlantic Meridional Overturning Circulation (AMOC) in CMIP5 Models: RCP and Historical Simulations, Journal of Climate, 26, 7187–7197, https://doi.org/10.1175/JCLI-D-12-00496.1, 2013.

Crueger, T., E., R., T., R., Schnur, R., and Wetzel, P.: Ocean dynamics determine the response of oceanic CO2 uptake to climate change., Climate Dynamics, 31, 151–168, https://doi.org/10.1007/s00382-007-0342-x, 2008.

Dunne, J. P., Horowitz, L. W., Adcroft, A. J., Ginoux, P., Held, I. M., John, J. G., Krasting, J. P., Malyshev, S., Naik, V., Paulot, F., Shevliakova, E., Stock, C. A., Zadeh, N., Balaji, V., Blanton, C., Dunne, K. A., Dupuis, C., Durachta, J., Dussin, R., Gauthier, P. P. G., Griffies, S. M., Guo, H., Hallberg, R. W., Harrison, M., He, J., Hurlin, W., McHugh, C., Menzel, R., Milly, P. C. D., Nikonov, S., Paynter, D. J., Ploshay, J., Radhakrishnan, A., Rand, K., Reichl, B. G., Robinson, T., Schwarzkopf, D. M., Sentman, L. T., Underwood, S., Vahlenkamp, H., Winton,

https://doi.org/10.5194/bg-2020-487
Preprint. Discussion started: 4 January 2021




M., Wittenberg, A. T., Wyman, B., Zeng, Y., and Zhao, M.: The GFDL Earth System Model Version 4.1 (GFDL-ESM 4.1): Overall Coupled Model Description and Simulation Characteristics, Journal of Advances in Modeling Earth Systems, 12, e2019MS002 015, https://doi.org/10.1029/2019MS002015, 2020.

595 Follows, M. J., Ito, T., and Dutkiewicz, S.: On the solution of the carbonate chemistry system in ocean biogeochemistry models, Ocean Modelling, 12, 290–301, https://doi.org/https://doi.org/10.1016/j.ocemod.2005.05.004, 2006.

Friedlingstein, P., Dufrense, J.-L., Cox, P. M., and Rayner, P.: How positive is the feedback between climate change and the carbon cycle?, Tellus B, 55, 692–700, https://doi.org/10.1034/j.1600-0889.2003.01461.x, 2003.

Friedlingstein, P., Cox, P., Betts, R., Bopp, L., von Bloh, W., Brovkin, V., Cadule, P., Doney, S., Eby, M., Fung, I., Bala, G., John, J., Jones,
600 C., Joos, F., Kato, T., Kawamiya, M., Knorr, W., Lindsay, K., Matthews, H. D., Raddatz, T., Rayner, P., Reick, C., Roeckner, E., Schnitzler, K.-G., Schnur, R., Strassmann, K., Weaver, A. J., Yoshikawa, C., and Zeng, N.: Climate-Carbon Cycle Feedback Analysis: Results from the C4MIP Model Intercomparison, Journal of Climate, 19, 3337–3353, https://doi.org/10.1175/JCLI3800.1, 2006.

Frölicher, T. L., Sarmiento, J. L., Paynter, D. J., Dunne, J. P., Krasting, J. P., and Winton, M.: Dominance of the Southern Ocean in Anthropogenic Carbon and Heat Uptake in CMIP5 Models, Journal of Climate, 28, 862–886, https://doi.org/10.1175/JCLI-D-14-00117.1,
605 2015.

Gnanadesikan, A.: A simple predictive model of the structure of the oceanic pycnocline, Science, 283, 2077–2081, https://doi.org/10.1126/science.283.5410.2077, 1999.

Gregory, J. M., Ingram, W. J., Palmer, M. A., Jones, G. S., Stott, P. A., Thorpe, R. B., Lowe, J. A., Johns, T. C., and Williams, K. D.: A new method for diagnosing radiative forcing and climate sensitivity, Geophysical Research Letters, 31, L03 205,
610 https://doi.org/10.1029/2003GL018747, 2004.

Gregory, J. M., Jones, C. D., Cadule, P., and Friedlingstein, P.: Quantifying Carbon Cycle Feedbacks, Journal of Climate, 22, 5232–5250, https://doi.org/10.1175/2009JCLI2949.1, https://doi.org/10.1175/2009JCLI2949.1, 2009.

Gruber, N., Sarmiento, J., and Stocker, T.: An improved method for detecting anthropogenic CO2 in the oceans, Global Biogeochemical Cycles, 10, 809–837, https://doi.org/10.1029/96GB01608, 1996.

615 Ito, T. and Follows, M. J.: Preformed phosphate, soft tissue pump and atmospheric CO2, Journal of Marine Research, 63, 813–839, https://doi.org/https://doi.org/10.1357/0022240054663231, 2005.

Ito, T., Bracco, A., Deutsch, C., Frenzel, H., Long, M., and Takano, Y.: Sustained growth of the Southern Ocean carbon storage in a warming climate, Geophysical Research Letters, 42, 4516–4522, https://doi.org/10.1002/2015GL064320, 2015.

Iudicone, D., Rodgers, K. B., Plancherel, Y., Aumont, O., Ito, T., Key, R. M., Madec, G., and Ishii, M.: The formation of the ocean's
620 anthropogenic carbon reservoir, Scientific Reports, 6, https://doi.org/10.1038/srep35473, 2016.

Johnson, H. L., Marshall, D. P., and Sproson, D. A. J.: Reconciling theories of a mechanically driven meridional overturning circulation with thermohaline forcing and multiple equilibria, Climate Dynamics, 29, 821–836, https://doi.org/10.1007/s00382-007-0262-9, 2007.

Jones, C. D., Arora, V., Friedlingstein, P., Bopp, L., Brovkin, V., Dunne, J., Graven, H., Hoffman, F., Ilyina, T., John, J. G., Jung, M., Kawamiya, M., Koven, C., Pongratz, J., Raddatz, T., Randerson, J. T., and Zaehle, S.: C4MIP-The Coupled Climate-
625 Carbon Cycle Model Intercomparison Project: experimental protocol for CMIP6, Geoscientific Model Development, 9, 2853–2880, https://doi.org/10.5194/gmd-9-2853-2016, https://gmd.copernicus.org/articles/9/2853/2016/, 2016.

Joos, F., Plattner, G.-K., Stocker, T. F., Marchal, O., and Schmittner, A.: Global Warming and Marine Carbon Cycle Feedbacks on Future Atmospheric CO2, Science, 284, 464–467, https://doi.org/10.1126/science.284.5413.464, 1999.

https://doi.org/10.5194/bg-2020-487
Preprint. Discussion started: 4 January 2021




Katavouta, A., Williams, R. G., Goodwin, P., and Roussenov, V.: Reconciling Atmospheric and Oceanic Views of the Transient Climate Response to Emissions, Geophysical Research Letters, 45, 6205–6214, https://doi.org/10.1029/2018GL077849, 2018.

Katavouta, A., Williams, R. G., and Goodwin, P.: The Effect of Ocean Ventilation on the Transient Climate Response to Emissions, Journal of Climate, 32, 5085–5105, https://doi.org/10.1175/JCLI-D-18-0829.1, 2019.

Khatiwala, S., Primeau, F., and Hall, T.: Reconstruction of the history of anthropogenic CO2 concentrations in the ocean, Nature, 462, 346–349, https://doi.org/10.1038/nature08526, 2009.

Lauderdale, J. M., Naveira-Garabato, A. C., Oliver, K. I. C., Follows, M. J., and Williams, R. G.: Wind-driven changes in Southern Ocean residual circulation, ocean carbon reservoirs and atmospheric CO2, Climate Dynamics, 41, 2145–2164, https://doi.org/10.1007/s00382-012-1650-3, 2013.

Marshall, D. P. and Zanna, L.: A Conceptual Model of Ocean Heat Uptake under Climate Change, Journal of Climate, 27, 8444–8465, https://doi.org/10.1175/JCLI-D-13-00344.1, 2014.

Marshall, J. and Speer, K.: Closure of the meridional overturning circulation through Southern Ocean upwelling, Nature Geoscience, 5, 171–180, https://doi.org/10.1038/ngeo1391, 2012.

Mauritsen, T., Bader, J., Becker, T., Behrens, J., Bittner, M., Brokopf, R., Brovkin, V., Claussen, M., Crueger, T., Esch, M., Fast, I., Fiedler, S., Fläschner, D., Gayler, V., Giorgetta, M., Goll, D. S., Haak, H., Hagemann, S., Hedemann, C., Hohenegger, C., Ilyina, T., Jahns, T., Jimenéz-de-la Cuesta, D., Jungclaus, J., Kleinen, T., Kloster, S., Kracher, D., Kinne, S., Kleberg, D., Lasslop, G., Kornblueh, L., Marotzke, J., Matei, D., Meraner, K., Mikolajewicz, U., Modali, K., Möbis, B., Müller, W. A., Nabel, J. E. M. S., Nam, C. C. W., Notz, D., Nyawira, S.-S., Paulsen, H., Peters, K., Pincus, R., Pohlmann, H., Pongratz, J., Popp, M., Raddatz, T. J., Rast, S., Redler, R., Reick, C. H., Rohrschneider, T., Schemann, V., Schmidt, H., Schnur, R., Schulzweida, U., Six, K. D., Stein, L., Stemmler, I., Stevens, B., von Storch, J.-S., Tian, F., Voigt, A., Vrese, P., Wieners, K.-H., Wilkenskjeld, S., Winkler, A., and Roeckner, E.: Developments in the MPI-M Earth System Model version 1.2 (MPI-ESM1.2) and Its Response to Increasing CO2, Journal of Advances in Modeling Earth Systems, 11, 998–1038, https://doi.org/10.1029/2018MS001400, 2019.

Meijers, A. J. S.: The Southern Ocean in the Coupled Model Intercomparison Project phase 5, Philosophical Transactions of the Royal Society A: Mathematical, Physical and Engineering Sciences, 372, 20130 296, https://doi.org/10.1098/rsta.2013.0296, 2014.

Mikaloff-Fletcher, S. E., Gruber, N., Jacobson, A. R., Doney, S. C., Dutkiewicz, S., Gerber, M., Follows, M., Joos, F., Lindsay, K., Menemenlis, D., Mouchet, A., Müller, S. A., and Sarmiento, J. L.: Inverse estimates of anthropogenic CO2 uptake, transport, and storage by the ocean, Global Biogeochemical Cycles, 20, https://doi.org/10.1029/2005GB002530, 2006.

Myhre, G., Highwood, E. J., Shine, K. P., and Stordal, F.: New estimates of radiative forcing due to well mixed greenhouse gases, Geophysical Research Letters, 25, 2715–2718, https://doi.org/10.1029/98GL01908, 1998.

Rodgers, K. B., Ishii, M., Frölicher, T. L., Schlunegger, S., Aumont, O., Toyama, K., and Slater, R. D.: Coupling of Surface Ocean Heat and Carbon Perturbations over the Subtropical Cells under Twenty-First Century Climate Change, Journal of Climate, 33, 10 321–10 338, https://doi.org/10.1175/JCLI-D-19-1022.1, 2020.

Roy, T., Bopp, L., Gehlen, M., Schneider, B., Cadule, P., Frölicher, T. L., Segschneider, J., Tjiputra, J., Heinze, C., and Joos, F.: Regional Impacts of Climate Change and Atmospheric CO2 on Future Ocean Carbon Uptake: A Multimodel Linear Feedback Analysis, Journal of Climate, 24, 2300–2318, https://doi.org/10.1175/2010JCLI3787.1, 2011.

Roy, T., Sallée, J. B., Bopp, L., and Metzl, N.: Diagnosing human-induced feedbacks between the Southern Ocean carbon cycle and the climate system: A multiple Earth System Model analysis, Journal of Climate, submitted, 2020.

https://doi.org/10.5194/bg-2020-487
Preprint. Discussion started: 4 January 2021




Sabine, C. L., Feely, R. A., Gruber, N., Key, R. M., Lee, K., Bullister, J. L., Wanninkhof, R., Wong, C. S., Wallace, D. W. R., Tilbrook, B., Millero, F. J., Peng, T.-H., Kozyr, A., Ono, T., and Rios, A. F.: The Oceanic Sink for Anthropogenic CO2, Science, 305, 367–371, https://doi.org/10.1126/science.1097403, 2004.

Sallée, J., Matear, R., and Rintoul, S.: Localized subduction of anthropogenic carbon dioxide in the Southern Hemisphere oceans, Nature Geoscience, 5, 579–584, https://doi.org/10.1038/ngeo1523, 2012.

Sallée, J.-B., Shuckburgh, E., Bruneau, N., Meijers, A. J. S., Bracegirdle, T. J., Wang, Z., and Roy, T.: Assessment of Southern Ocean water mass circulation and characteristics in CMIP5 models: Historical bias and forcing response, Journal of Geophysical Research: Oceans, 118, 1830–1844, https://doi.org/https://doi.org/10.1002/jgrc.20135, 2013.

Sarmiento, J. L. and Le Quéré, C.: Oceanic Carbon Dioxide Uptake in a Model of Century-Scale Global Warming, Science, 274, 1346–1350, https://doi.org/10.1126/science.274.5291.1346, 1996.

Sarmiento, J. L., Hughes, T., Stouffer, R., and Manabe, S.: Simulated response of the ocean carbon cycle to anthropogenic climate warming, Nature, 393, 245–249, https://doi.org/10.1038/30455, 1998.

Schwinger, J. and Tjiputra, J.: Ocean Carbon Cycle Feedbacks Under Negative Emissions, Geophysical Research Letters, 45, 5062–5070, https://doi.org/10.1029/2018GL077790, 2018.

Schwinger, J., Tjiputra, J. F., Heinze, C., Bopp, L., Christian, J., Gehlen, M., Ilyina, T., Jones, C., Salas-Mélia, D., Segschneider, J., Séférian, R., and Totterdell, I.: Nonlinearity of Ocean Carbon Cycle Feedbacks in CMIP5 Earth System Models, Journal of Climate, 27, 3869–3888, https://doi.org/10.1175/JCLI-D-13-00452.1, 2014.

Séférian, R., Nabat, P., Michou, M., Saint-Martin, D., Voldoire, A., Colin, J., Decharme, B., Delire, C., Berthet, S., Chevallier, M., Sénési, S., Franchisteguy, L., Vial, J., Mallet, M., Joetzjer, E., Geoffroy, O., Guérémy, J.-F., Moine, M.-P., Msadek, R., Ribes, A., Rocher, M., Roehrig, R., Salas-y Mélia, D., Sanchez, E., Terray, L., Valcke, S., Waldman, R., Aumont, O., Bopp, L., Deshayes, J., Éthé, C., and Madec, G.: Evaluation of CNRM Earth System Model, CNRM-ESM2-1: Role of Earth System Processes in Present-Day and Future Climate, Journal of Advances in Modeling Earth Systems, 11, 4182–4227, https://doi.org/10.1029/2019MS001791, 2019.

Séférian, R., Berthet, S., Yool, A., Palmiéri, J., Bopp, L., Tagliabue, A., Kwiatkowski, L., Aumont, O., Christian, J., Dunne, J., Gehlen, M., Ilyina, T., John, J., Li, H., Long, M., Luo, J., Nakano, H., Romanou, A., Schwinger, J., Stock, C., Santana-Falcón, Y., Takano, Y., Tjiputra, J., Tsujino, H., Watanabe, M., Wu, T., Wu, F., and Yamamoto, A.: Tracking improvement in simulated marine biogeochemistry between CMIP5 and CMIP6, Current Climate Change Reports, 17, 95?119, https://doi.org/10.1007/s40641-020-00160-0, 2020.

Seland, Ø., Bentsen, M., Seland Graff, L., Olivié, D., Toniazzo, T., Gjermundsen, A., Debernard, J. B., Gupta, A. K., He, Y., Kirkevåg, A., Schwinger, J., Tjiputra, J., Schancke Aas, K., Bethke, I., Fan, Y., Griesfeller, J., Grini, A., Guo, C., Ilicak, M., Hafsahl Karset, I. H., Landgren, O., Liakka, J., Onsum Moseid, K., Nummelin, A., Spensberger, C., Tang, H., Zhang, Z., Heinze, C., Iverson, T., and Schulz, M.: The Norwegian Earth System Model, NorESM2 – Evaluation of the CMIP6 DECK and historical simulations, Geoscientific Model Development Discussions, 2020, 1–68, https://doi.org/10.5194/gmd-2019-378, https://gmd.copernicus.org/preprints/gmd-2019-378/, 2020.

Sellar, A. A., Jones, C. G., Mulcahy, J. P., Tang, Y., Yool, A., Wiltshire, A., O'Connor, F. M., Stringer, M., Hill, R., Palmieri, J., Woodward, S., de Mora, L., Kuhlbrodt, T., Rumbold, S. T., Kelley, D. I., Ellis, R., Johnson, C. E., Walton, J., Abraham, N. L., Andrews, M. B., Andrews, T., Archibald, A. T., Berthou, S., Burke, E., Blockley, E., Carslaw, K., Dalvi, M., Edwards, J., Folberth, G. A., Gedney, N., Griffiths, P. T., Harper, A. B., Hendry, M. A., Hewitt, A. J., Johnson, B., Jones, A., Jones, C. D., Keeble, J., Liddicoat, S., Morgenstern, O., Parker, R. J., Predoi, V., Robertson, E., Siahaan, A., Smith, R. S., Swaminathan, R., Woodhouse, M. T., Zeng, G., and Zerroukat, M.: UKESM1: Description and Evaluation of the U.K. Earth System Model, Journal of Advances in Modeling Earth Systems, 11, 4513–4558, https://doi.org/0.1029/2019MS001739, 2019.

https://doi.org/10.5194/bg-2020-487
Preprint. Discussion started: 4 January 2021




Sherwood, S. C., Bony, S., Boucher, O., Bretherton, C., Forster, P. M., Gregory, J. M., and Stevens, B.: Adjustments in the Forcing-Feedback Framework for Understanding Climate Change, Bulletin of the American Meteorological Society, 96, 217–228, https://doi.org/10.1175/BAMS-D-13-00167.1, 2015.

Swart, N. C., Cole, J. N. S., Kharin, V. V., Lazare, M., Scinocca, J. F., Gillett, N. P., Anstey, J., Arora, V., Christian, J. R., Hanna, S., Jiao, Y., Lee, W. G., Majaess, F., Saenko, O. A., Seiler, C., Seinen, C., Shao, A., Sigmond, M., Solheim, L., von Salzen, K., Yang, D., and Winter, B.: The Canadian Earth System Model version 5 (CanESM5.0.3), Geoscientific Model Development, 12, 4823–4873, https://doi.org/10.5194/gmd-12-4823-2019, 2019.

Tjiputra, J. F., Assmann, K., Bentsen, M., Bethke, I., Otterå, O. H., Sturm, C., and Heinze, C.: Bergen Earth system model (BCM-C): model description and regional climate-carbon cycle feedbacks assessment, Geoscientific Model Development, 3, 123–141, https://doi.org/10.5194/gmd-3-123-2010, 2010.

Williams, R., Katavouta, A., and Goodwin, P.: Carbon-Cycle Feedbacks Operating in the Climate System, Current Climate Change Report, 5, 282–295, https://doi.org/10.1007/s40641-019-00144-9, 2019.

Williams, R., Katavouta, A., and Roussenov, V.: Regional asymmetries in ocean heat and carbon storage due to dynamic redistribution in climate model projections, Journal of Climate, in review, 2020.

Williams, R. G. and Follows, M. J.: Ocean Dynamics and the Carbon Cycle: Principles and Mechanisms, Cambridge University Press, 2011.

Winton, M., Griffies, S. M., Samuels, B. L., Sarmiento, J. L., and Frölicher, T. L.: Connecting Changing Ocean Circulation with Changing Climate, Journal of Climate, 26, 2268–2278, https://doi.org/10.1175/JCLI-D-12-00296.1, 2013.

Yoshikawa, C., Kawamiya, M., Kato, T., Yamanaka, Y., and Matsuno, T.: Geographical distribution of the feedback between future climate change and the carbon cycle, Journal of Geophysical Research: Biogeosciences, 113, https://doi.org/10.1029/2007JG000570, 2008.

Yukimoto, S., Kawai, H., Koshiro, T., Oshima, N., Yoshida, K., Urakawa, S., Tsujino, H., Deushi, M., Tanaka, T., Hosaka, M., Yabu, S., Yoshimura, H., Shindo, E., Mizuta, R., Obata, A., Adachi, Y., and Ishii, M.: The Meteorological Research Institute Earth System Model Version 2.0, MRI-ESM2.0: Description and Basic Evaluation of the Physical Component, Journal of the Meteorological Society of Japan. Ser. II, 97, 931–965, https://doi.org/10.2151/jmsj.2019-051, 2019.

Zickfeld, K., Eby, M., and Weaver, A. J.: Carbon-cycle feedbacks of changes in the Atlantic meridional overturning circulation under future atmospheric CO2, Global Biogeochemical Cycles, 22, https://doi.org/10.1029/2007GB003118, 2008.

Zickfeld, K., Eby, M., Matthews, H. D., Schmittner, A., and Weaver, A. J.: Nonlinearity of Carbon Cycle Feedbacks, Journal of Climate, 24, 4255–4275, https://doi.org/10.1175/2011JCLI3898.1, https://doi.org/10.1175/2011JCLI3898.1, 2011.

Ziehn, T., Chamberlain, M., Law, R., Lenton, A., Bodman, R., Dix, M., Stevens, L., Wang, Y.-P., and Jhan, J. S.: The Australian Earth System Model: ACCESS-ESM1.5, Journal of Southern Hemisphere Earth Systems Science, https://doi.org/10.1071/ES19035, 2020.

https://doi.org/10.5194/bg-2020-487
Preprint. Discussion started: 4 January 2021



**Table 1.** List of the 10 CMIP6 Earth system models used in this study along with references for the model description.

| Earth system model | Reference |
|---|---|
| ACCESS-ESM1.5 | Ziehn et al. (2020) |
| CanESM5 | Swart et al. (2019) |
| CanESM5-CanOE | Swart et al. (2019) |
| CNRM-ESM2-1 | Séférian et al. (2019) |
| GFDL-ESM4 | Dunne et al. (2020) |
| IPSL-CM6A-LR | Boucher et al. (2020) |
| MPI-ESM1.2-LR | Mauritsen et al. (2019) |
| MRI-ESM2 | Yukimoto et al. (2019) |
| NorESM2-LM | Seland et al. (2020) |
| UKESM1-0-LL | Sellar et al. (2019) |

https://doi.org/10.5194/bg-2020-487
Preprint. Discussion started: 4 January 2021


Biogeosciences Discussions

**Table 2.** Carbon-concentration feedback parameter, $\beta$ (PgC ppm$^{-1}$), and carbon-climate feedback parameter, $\gamma$ (PgC $^{o}$C$^{-1}$), for the global ocean and different ocean basins in 10 CMIP6 Earth system models, along with the inter-model mean, standard deviation and coefficient of variation (CV), estimated as the standard deviation divided by the mean. The estimates are based on the fully coupled simulation (COU) and the biogeochemically coupled simulation (BGC) under the 1% yr$^{-1}$ increasing $CO_2$ experiment. The control run is used to estimate the changes relative to the pre-industrial to exclude model biases. Diagnostics are from years 121 to 140 (the 20 years up to quadrupling of atmospheric $CO_2$).

| Parameter $\beta$ | | | | | |
|---|---|---|---|---|---|
| model | $\beta_{ocean}$ | $\beta_{Atlantic}$ | $\beta_{Indian}$ | $\beta_{Pacific}$ | $\beta_{Southern}$ |
| ACCESS-ESM1.5 | 0.901 | 0.241 | 0.099 | 0.247 | 0.277 |
| CanESM5 | 0.794 | 0.192 | 0.098 | 0.256 | 0.210 |
| CanESM5-CanOE | 0.750 | 0.178 | 0.094 | 0.241 | 0.202 |
| CNRM-ESM2-1 | 0.794 | 0.210 | 0.103 | 0.251 | 0.191 |
| GFDL-ESM4 | 0.933 | 0.257 | 0.107 | 0.278 | 0.250 |
| IPSL-CM6A-LR | 0.777 | 0.192 | 0.101 | 0.249 | 0.201 |
| MPI-ESM1.2-LR | 0.803 | 0.211 | 0.085 | 0.237 | 0.235 |
| MRI-ESM2 | 0.966 | 0.258 | 0.121 | 0.306 | 0.235 |
| NorESM2-LM | 0.815 | 0.236 | 0.088 | 0.197 | 0.252 |
| UKESM1-0-LL | 0.736 | 0.203 | 0.102 | 0.198 | 0.192 |
| mean | 0.827 | 0.218 | 0.100 | 0.246 | 0.225 |
| std | 0.079 | 0.028 | 0.010 | 0.033 | 0.030 |
| CV | 0.096 | 0.128 | 0.100 | 0.134 | 0.133 |
| Parameter $\gamma$ | | | | | |
| model | $\gamma_{ocean}$ | $\gamma_{Atlantic}$ | $\gamma_{Indian}$ | $\gamma_{Pacific}$ | $\gamma_{Southern}$ |
| ACCESS-ESM1.5 | -20.56 | -3.34 | -1.15 | -8.79 | -6.40 |
| CanESM5 | -13.94 | -2.65 | -1.94 | -5.41 | -2.59 |
| CanESM5-CanOE | -11.21 | -2.16 | -1.26 | -4.40 | -2.22 |
| CNRM-ESM2-1 | -1.54 | -0.04 | 0.61 | -2.16 | 0.90 |
| GFDL-ESM4 | -18.41 | -6.35 | -5.70 | -2.06 | -2.58 |
| IPSL-CM6A-LR | -11.82 | -3.07 | -1.03 | -4.76 | -2.28 |
| MPI-ESM1.2-LR | -16.70 | -5.99 | -1.19 | -2.77 | -5.39 |
| MRI-ESM2 | -27.64 | -12.19 | -1.64 | -10.42 | 0.19 |
| NorESM2-LM | -18.00 | -6.13 | -0.13 | -2.43 | -8.35 |
| UKESM1-0-LL | -11.94 | -3.28 | -2.05 | -2.84 | -2.23 |
| mean | -15.18 | -4.52 | -1.18 | -4.97 | -3.10 |
| std | 6.91 | 3.35 | 0.86 | 2.77 | 2.85 |
| CV | 0.46 | 0.74 | 0.73 | 0.56 | 0.92 |

https://doi.org/10.5194/bg-2020-487
Preprint. Discussion started: 4 January 2021


Biogeosciences Discussions

**Table 3.** Carbon-concentration feedback parameter, $\beta$ (PgC ppm$^{-1}$), and carbon-climate feedback parameter, $\gamma$ (PgC $^{o}$C$^{-1}$), in the Atlantic Ocean, and the contribution from the saturated, disequilibrium and regenerated carbon pools, along with the strength of the Atlantic Meridional Overturning Circulation, AMOC in $Sv$, at the pre-industrial and its weakening relative to the pre-industrial due to climate change. The strength and weakening of the AMOC are for the maximum pre-industrial AMOC and maximum AMOC change between 30$^{o}$N to 50$^{o}$N, respectively (Figs 7 and 8). Results are shown for 10 CMIP6 Earth system models, along with the inter-model mean, standard deviation and coefficient of variation (CV), estimated as the standard deviation divided by the mean. The estimates are based on the fully coupled simulation (COU) and the biogeochemically coupled simulation (BGC) under the 1% yr$^{-1}$ increasing $CO_2$ experiment. The control run was used to estimate the changes relative to the pre-industrial to exclude model biases. Diagnostics are from years 121 to 140 (the 20 years up to quadrupling of atmospheric $CO_2$).

| Parameter $\beta$ | | | | | |
|---|---|---|---|---|---|
| model | pre-industrial AMOC | $\beta$ | $\beta_{sat}$ | $\beta_{dis}$ | $\beta_{reg}$ |
| ACCESS-ESM1.5 | 22.24 | 0.241 | 0.723 | -0.482 | 0.000 |
| CanESM5 | 13.16 | 0.192 | 0.763 | -0.571 | 0.000 |
| CanESM5-CanOE | 12.23 | 0.178 | 0.721 | -0.542 | 0.000 |
| CNRM-ESM2-1 | 16.41 | 0.210 | 0.741 | -0.543 | 0.012 |
| GFDL-ESM4 | 21.74 | 0.257 | 0.756 | -0.513 | 0.014 |
| IPSL-CM6A-LR | 11.32 | 0.192 | 0.731 | -0.539 | 0.000 |
| MPI-ESM1.2-LR | 22.36 | 0.211 | 0.730 | -0.519 | 0.000 |
| MRI-ESM2 | 22.50 | 0.258 | 0.743 | -0.485 | 0.000 |
| NorESM2-LM | 23.18 | 0.236 | 0.751 | -0.515 | 0.000 |
| UKESM1-0-LL | 15.61 | 0.203 | 0.725 | -0.526 | 0.004 |
| mean | 18.08 | 0.218 | 0.738 | -0.524 | 0.003 |
| std | 4.80 | 0.028 | 0.015 | 0.027 | 0.005 |
| CV | 0.27 | 0.128 | 0.020 | 0.052 | 1.667 |
| Parameter $\gamma$ | | | | | |
| model | AMOC weakening | $\gamma$ | $\gamma_{sat}$ | $\gamma_{dis}$ | $\gamma_{reg}$ |
| ACCESS-ESM1.5 | -7.04 | -3.34 | -0.17 | -4.49 | 1.32 |
| CanESM5 | -5.48 | -2.65 | -0.32 | -2.79 | 0.47 |
| CanESM5-CanOE | -4.90 | -2.16 | -0.66 | -2.56 | 1.06 |
| CNRM-ESM2-1 | -7.71 | -0.04 | -2.57 | -4.94 | 7.46 |
| GFDL-ESM4 | -12.04 | -6.35 | -1.11 | -7.70 | 2.47 |
| IPSL-CM6A-LR | -3.60 | -3.07 | -2.00 | -4.18 | 3.11 |
| MPI-ESM1.2-LR | -7.95 | -5.99 | -2.17 | -5.73 | 1.91 |
| MRI-ESM2 | -17.47 | -12.19 | -1.84 | -14.25 | 3.90 |
| NorESM2-LM | -12.45 | -6.13 | -1.93 | -7.06 | 2.86 |
| UKESM1-0-LL | -6.92 | -3.28 | -0.80 | -3.56 | 1.08 |
| mean | -8.56 | -4.52 | -1.36 | -5.73 | 2.56 |
| std | 4.22 | 3.35 | 0.85 | 3.44 | 2.03 |
| CV | 0.49 | 0.74 | 0.63 | 0.60 | 0.79 |

https://doi.org/10.5194/bg-2020-487
Preprint. Discussion started: 4 January 2021


Biogeosciences Discussions Open Access EGU

**Table 4.** Correlation between the ocean carbon-concentration feedback parameter, $\beta$, and the pre-industrial strength of the Atlantic Meridional Overturning Circulation (AMOC) and correlation between the ocean carbon-climate feedback parameter, $\gamma$ and the AMOC weakening due to climate change, along with the contribution from the saturated, disequilibrium and regenerated carbon pools based on 10 CMIP6 models (Table 1). For the regenerated part of $\gamma$, correlations estimated excluding the CNRM-ESM2-1 model, which has substantially larger changes in the regenerated carbon with warming than the rest of the Earth system models, are presented as $\widehat{\gamma}_{reg}$. The correlation is expressed as a correlation coefficient, $r$, and a $p$-value. The level of significance is assumed as 0.05 and the statistically significant correlations with $p$<0.05 are highlighted by bold text. Diagnostics are from years 121 to 140 (the 20 years up to quadrupling of atmospheric $CO_2$).

| $r$ and $p$-value for correlation between $\beta$ and pre-industrial AMOC strength | | | | | |
|---|---|---|---|---|---|
| ocean basin | $\beta$ | $\beta_{sat}$ | $\beta_{dis}$ | $\beta_{reg}$ | |
| Global Ocean | $r$=**0.70**, $p$=**0.025** | $r$=-0.06, $p$=0.879 | $r$=0.48, $p$=0.161 | $r$=0.20, $p$=0.570 | |
| Atlantic Ocean | $r$=**0.87**, $p$=**0.001** | $r$=0.18, $p$=0.628 | $r$=**0.79**, $p$=**0.006** | $r$=0.10, $p$=0.790 | |
| Indian Ocean | $r$=0.03, $p$=0.945 | $r$=-0.31, $p$=0.389 | $r$=0.27, $p$=0.455 | $r$=-0.09, $p$=0.812 | |
| Pacific Ocean | $r$=0.12, $p$=0.741 | $r$=-0.07, $p$=0.842 | $r$=0.10, $p$=0.778 | $r$=0.24, $p$=0.508 | |
| Southern Ocean | $r$=**0.82**, $p$=**0.004** | $r$=-0.04, $p$=0.919 | $r$=0.56, $p$=0.095 | $r$=0.26, $p$=0.474 | |
| $r$ and $p$-value for correlation between $\gamma$ and AMOC weakening with climate change | | | | | |
| ocean basin | $\gamma$ | $\gamma_{sat}$ | $\gamma_{dis}$ | $\gamma_{reg}$ | $\widehat{\gamma}_{reg}$ |
| Global Ocean | $r$=**0.67**, $p$=**0.034** | $r$=0.53, $p$=0.113 | $r$=**0.76**, $p$=**0.011** | $r$=-0.08, $p$=0.833 | $r$=-0.34 $p$=0.378 |
| Atlantic Ocean | $r$=**0.86**, $p$=**0.001** | $r$=0.29, $p$=0.408 | $r$=**0.94**, $p$<**0.001** | $r$=-0.29, $p$=0.412 | $r$=**-0.67** $p$=**0.049** |
| Indian Ocean | $r$=0.04, $p$=0.912 | $r$=0.16, $p$=0.651 | $r$=-0.07, $p$=0.858 | $r$=0.02, $p$=0.959 | $r$=-0.09 $p$=0.818 |
| Pacific Ocean | $r$=0.42, $p$=0.225 | $r$=0.41, $p$=0.242 | $r$=0.04, $p$=0.918 | $r$=0.52, $p$=0.120 | $r$=0.66 $p$=0.054 |
| Southern Ocean | $r$=-0.03, $p$=0.931 | $r$=0.01, $p$=0.986 | $r$=0.24, $p$=0.499 | $r$=-0.23, $p$=0.520 | $r$=-0.41 $p$=0.271 |

https://doi.org/10.5194/bg-2020-487
Preprint. Discussion started: 4 January 2021


Biogeosciences
Discussions
Open Access
EGU

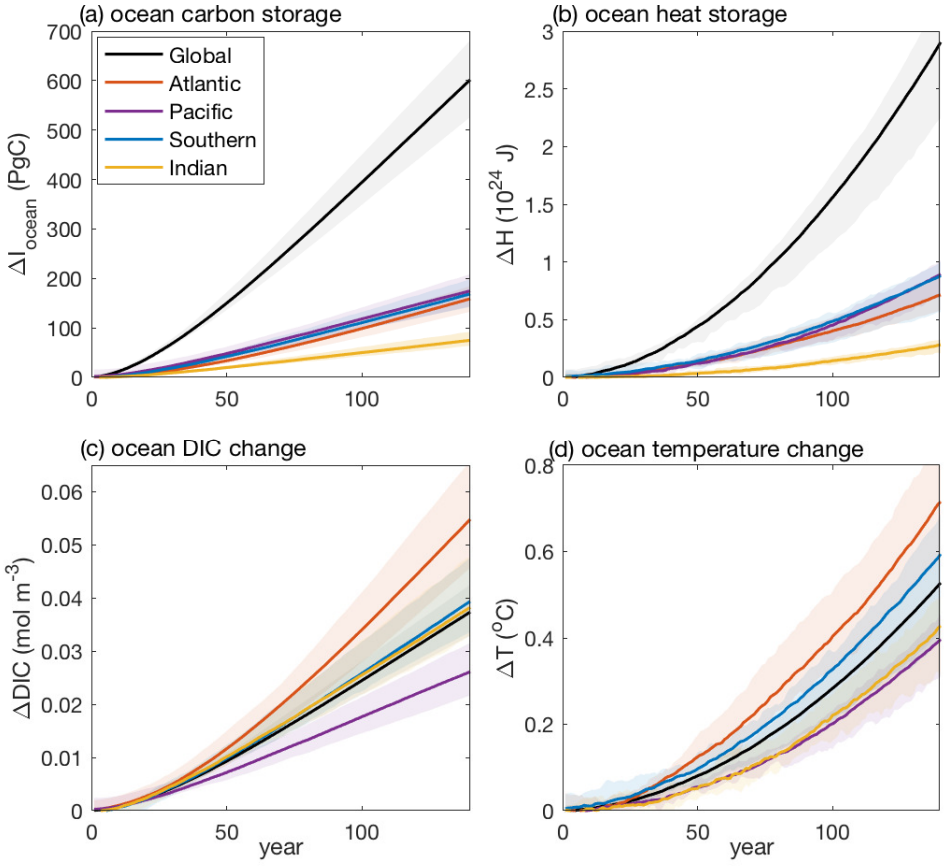


**Figure 1.** Carbon and heat storage for the global ocean and different ocean basins in CMIP6 Earth system models: (a) ocean carbon content changes relative to the pre-industrial in PgC, (b) ocean heat content changes relative to the pre-industrial in J, (c) changes in the ocean dissolved inorganic carbon relative to the pre-industrial in mol $m^{-3}$, expressing the ocean carbon storage changes per volume; and (d) changes in ocean temperature relative to the pre-industrial in $^{o}$C, expressing the ocean heat changes per volume. The solid lines show the model mean and the shading the model range based on the the 1 % $yr^{-1}$ increasing $CO_2$ experiment over 140 years in 10 CMIP6 models (Table 1). The control run was used to estimate the changes relative to the pre-industrial to exclude model biases.

https://doi.org/10.5194/bg-2020-487
Preprint. Discussion started: 4 January 2021


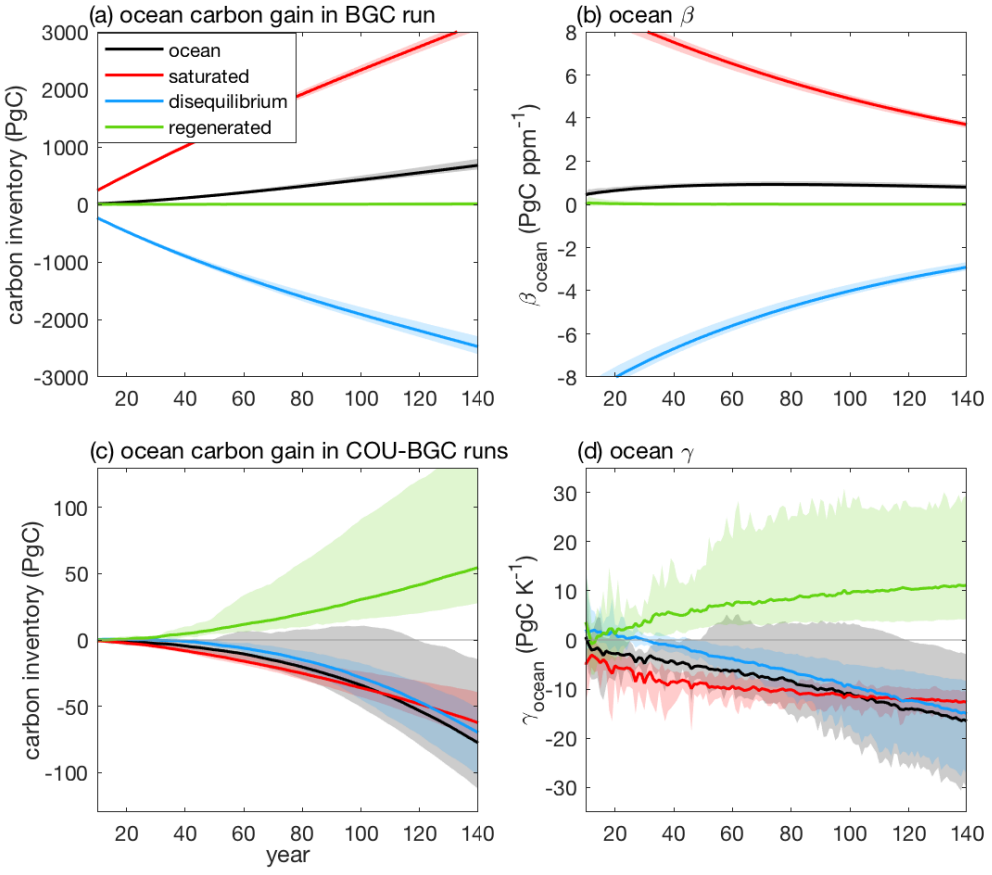


**Figure 2.** Ocean carbon storage relative to the pre-industrial and ocean carbon cycle feedback parameters $\beta_{ocean}$ and $\gamma_{ocean}$, along with the contribution from the saturated, disequilibrium and regenerated carbon pools in CMIP6 Earth system models: (a) ocean carbon inventory changes in the biogeochemically coupled simulation (BGC); (b) ocean carbon-concentration feedback parameter, $\beta_{ocean}$ (PgC ppm$^{-1}$); (c) ocean carbon inventory changes in the fully coupled simulation (COU) minus the biogeochemically coupled simulation (BGC); and (d) ocean carbon-climate feedback parameter, $\gamma_{ocean}$ (PgC K$^{-1}$). The solid lines show the model mean and the shading the model range based on the the 1 % yr$^{-1}$ increasing $CO_2$ experiment over 140 years in 10 CMIP6 models (Table 1). The feedback parameters are based on the fully coupled simulation (COU) and the biogeochemically coupled simulation (BGC) .The control run was used to estimate the changes relative to the pre-industrial to exclude model biases.

https://doi.org/10.5194/bg-2020-487
Preprint. Discussion started: 4 January 2021


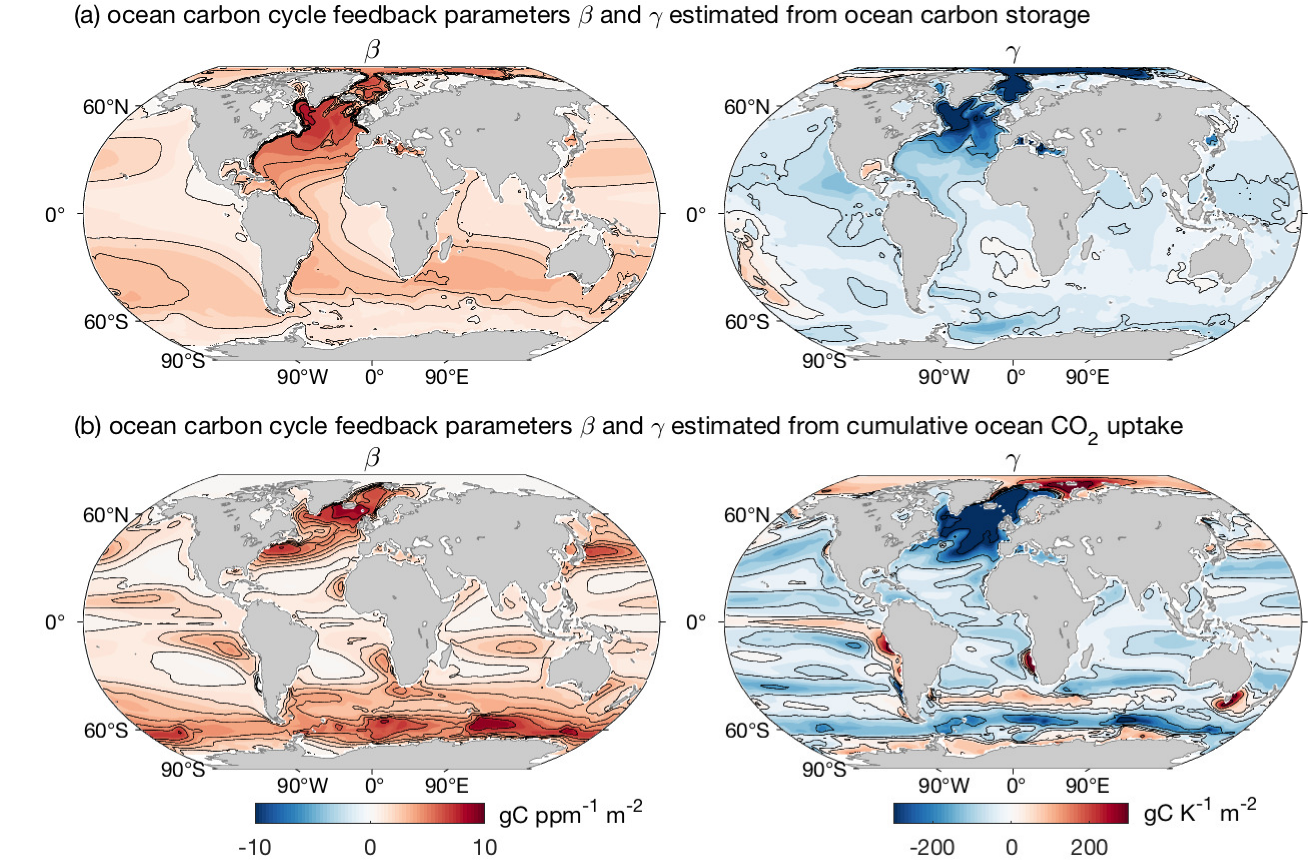


**Figure 3.** Geographical distribution of the CMIP6 inter-model mean carbon cycle feedback parameters normalised by area, $\beta$ (gC ppm$^{-1}$ m$^{-2}$) and $\gamma$ (gC K$^{-1}$ m$^{-2}$), as estimated: (a) based on the regional ocean carbon inventory changes; and (b) based on the regional cumulative ocean carbon uptake from the atmosphere. The estimates are based on the fully coupled simulation (COU) and the biogeochemically coupled simulation (BGC) under the 1% yr$^{-1}$ increasing $CO_2$ experiment. The control run was used to estimate the changes relative to the pre-industrial to exclude model biases. Diagnostics are from years 121 to 140 (the 20 years up to quadrupling of atmospheric $CO_2$). The intermodel mean is based on the models in Table 1 excluding NorESM2-LM for which the air-sea carbon flux for the BGC run was not available.

https://doi.org/10.5194/bg-2020-487
Preprint. Discussion started: 4 January 2021


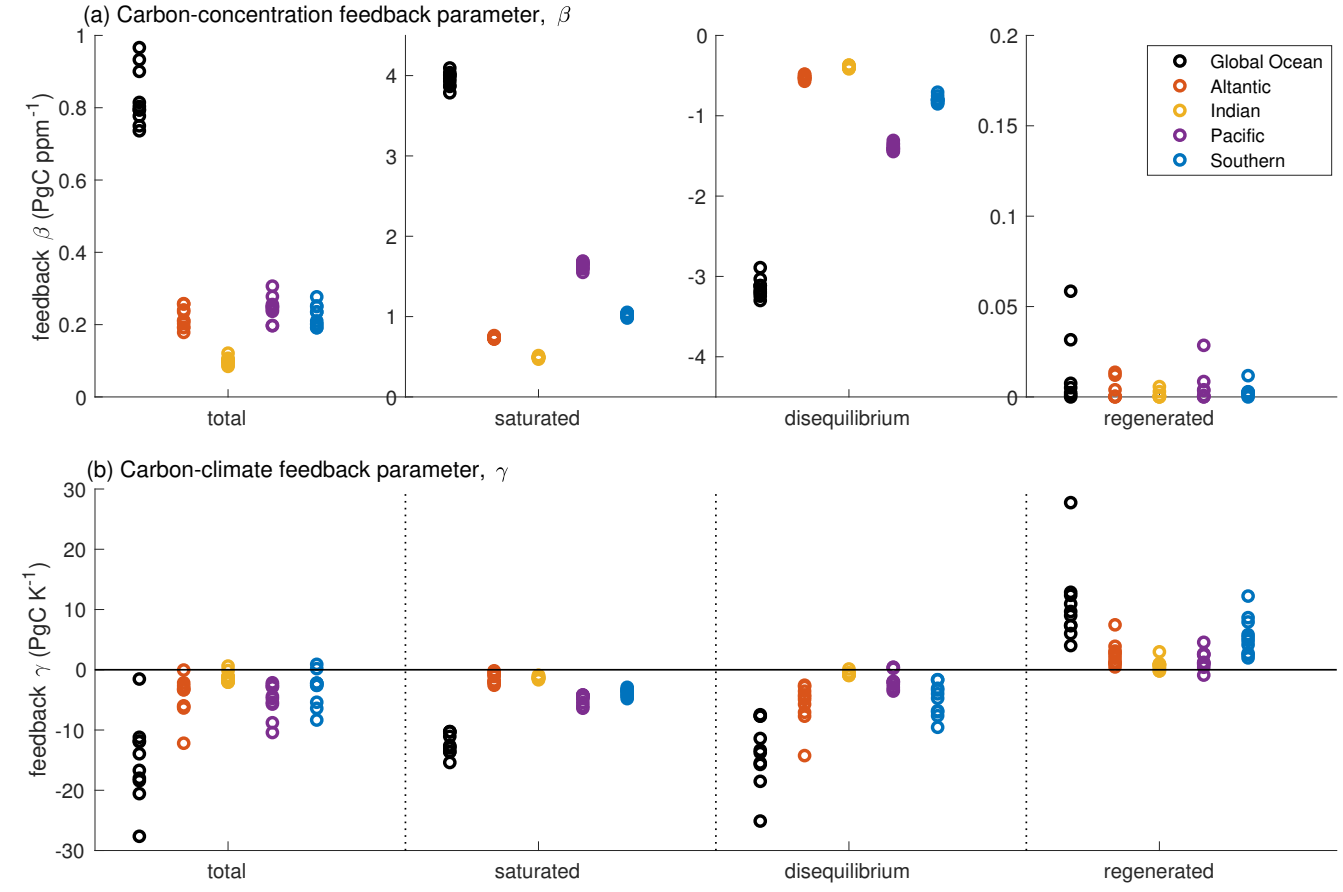


**Figure 4.** Carbon cycle feedback parameters along with the contribution from the saturated, disequilibrium and regenerated carbon pools, for the global ocean and the different ocean basins in 10 CMIP6 Earth system models (Table 1): (a) carbon-concentration feedback parameter, $\beta$ (PgC ppm$^{-1}$), and (b) carbon-climate feedback parameter $\gamma$ (PgC K$^{-1}$). The estimates are based on the fully coupled simulation (COU) and the biogeochemically coupled simulation (BGC) under the 1% yr$^{-1}$ increasing $CO_2$ experiment. The control run was used to estimate the changes relative to the pre-industrial to exclude model biases. Diagnostics are from years 121 to 140 (the 20 years up to quadrupling of atmospheric $CO_2$).

https://doi.org/10.5194/bg-2020-487
Preprint. Discussion started: 4 January 2021


Biogeosciences
Discussions
Open Access
EGU

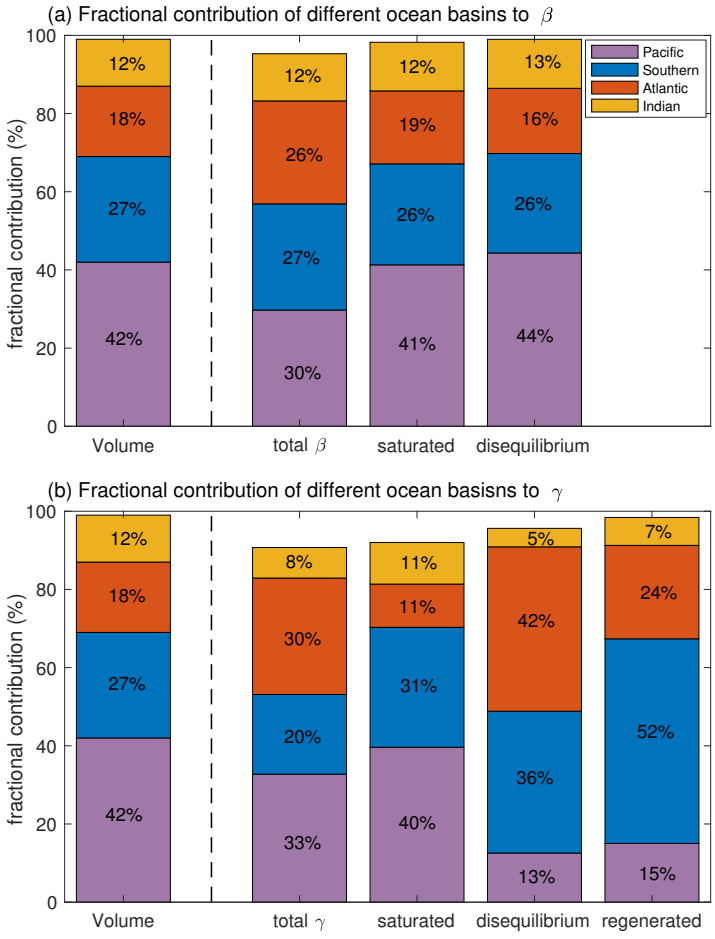


**Figure 5.** The fractional contribution (in %) of different ocean basins to the total volume of the ocean and to the ocean carbon cycle feedback parameters, along with the contribution from the saturated, disequilibrium and regenerated carbon pools based on the inter-model mean of 10 CMIP6 models (Table 1): (a) carbon-concentration feedback parameter, $\beta$, and (b) carbon-climate feedback parameter, $\gamma$. The estimates are based on the fully coupled simulation (COU) and the biogeochemically coupled simulation (BGC) under the 1% $yr^{-1}$ increasing $CO_2$ experiment. The control run was used to estimate the changes relative to the pre-industrial to exclude model biases. Diagnostics are from years 121 to 140 (the 20 years up to quadrupling of atmospheric $CO_2$). The regenerated part of $\beta$ is omitted as its contribution to $\beta$ is negligible in all basins (Fig. 4).

https://doi.org/10.5194/bg-2020-487
Preprint. Discussion started: 4 January 2021


Biogeosciences
Discussions
Open Access
EGU

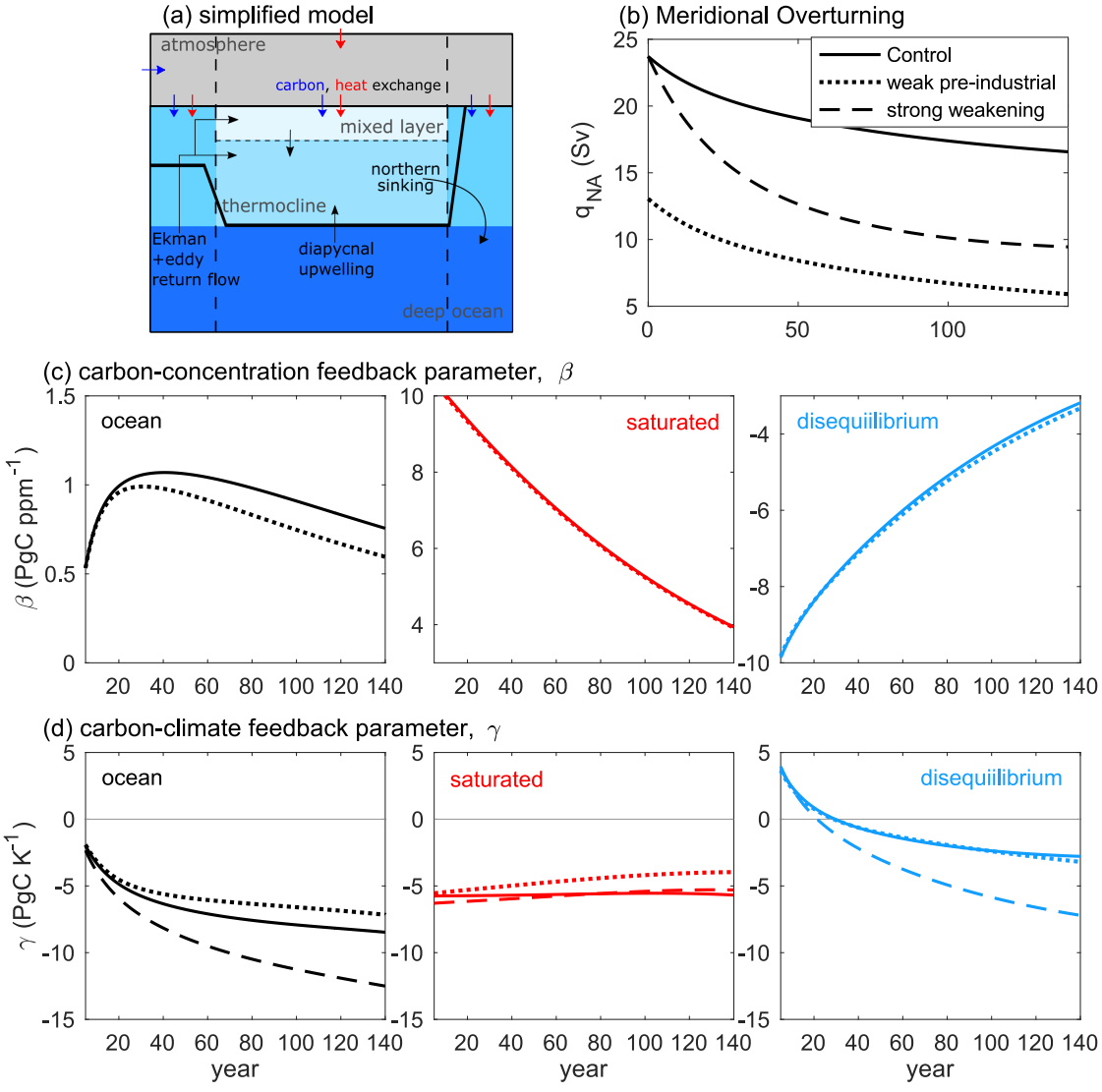


**Figure 6.** (a) A simplified climate model with overturning circulation, including a slab atmosphere, an upper layer of light water consisting of a thermocline layer and a surface mixed layer in the low and mid latitudes, two upper layers at southern and northern high latitudes, and a lower layer of dense water. (b) Meridional overturning in the three experiments forced by 1% yr$^{-1}$ increase in atmospheric $CO_2$: (i) control experiment (solid line), (ii) weaker pre-industrial overturning (dotted line), and (iii) larger reduction in the overturning with climate change. (c) The ocean carbon-concentration feedback parameter, $\beta$, and (c) the ocean carbon-climate feedback parameter, $\gamma$, along with their saturated and disequilibrium parts, in the experiments with different meridional overturning. The estimates of $\beta$ and $\gamma$ are based on the fully coupled simulations (COU) and the biogeochemically coupled simulations (BGC).

https://doi.org/10.5194/bg-2020-487
Preprint. Discussion started: 4 January 2021


Biogeosciences
Discussions
Open Access
EGU

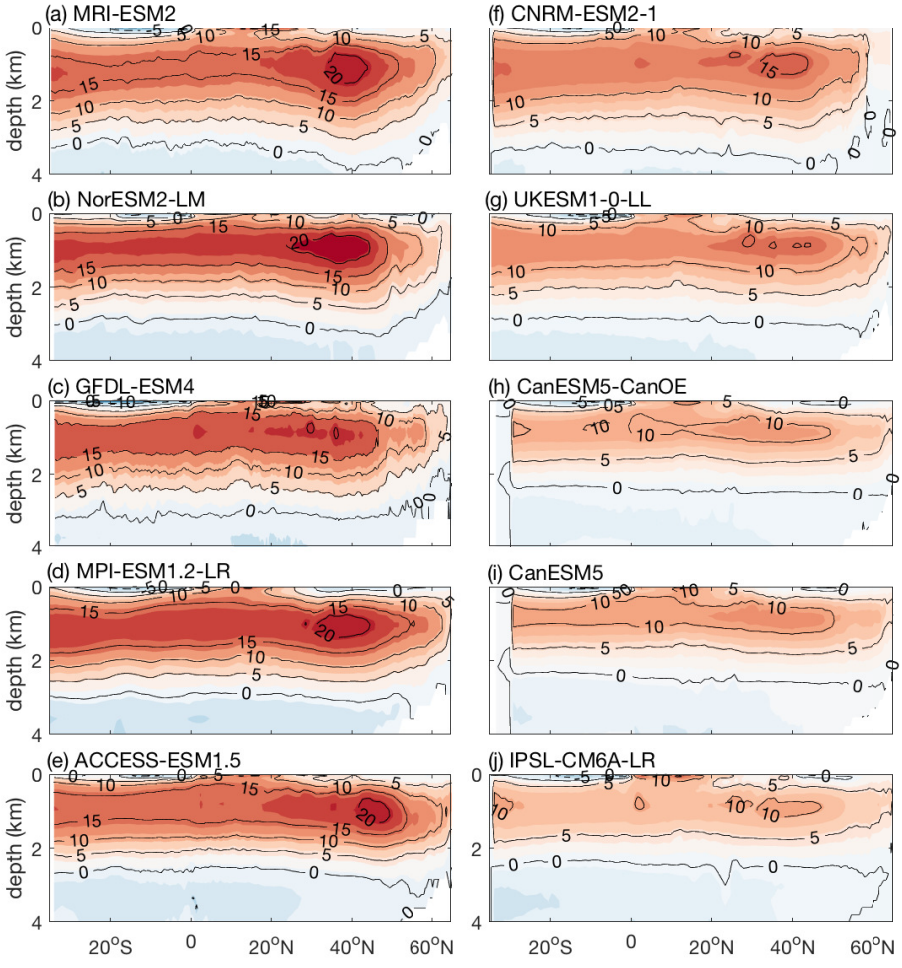


**Figure 7.** The Atlantic Meridional Overturning Circulation, AMOC ($Sv$), at the pre-industrial in 10 CMIP6 Earth system models. The estimates are based on the control run for years 121 to 140 to exclude model biases.

https://doi.org/10.5194/bg-2020-487
Preprint. Discussion started: 4 January 2021


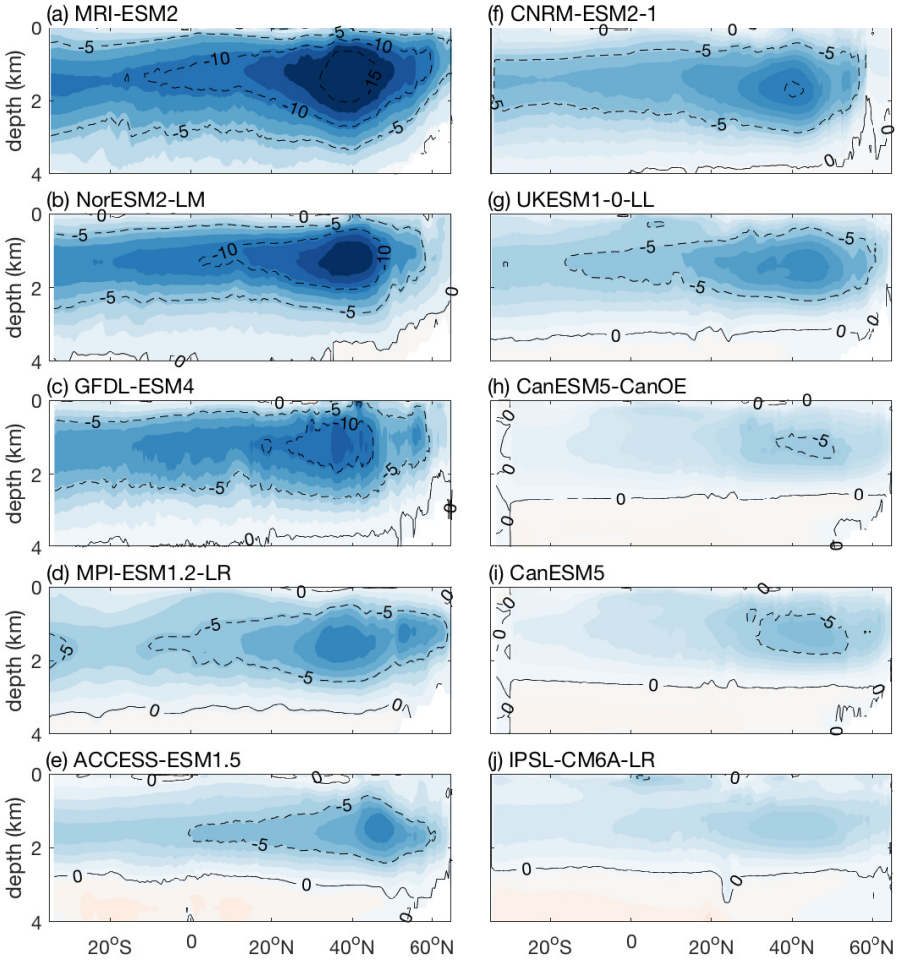


**Figure 8.** Weakening of the Atlantic Meridional Overturning Circulation, AMOC ($Sv$), relative to the pre-industrial in 10 CMIP6 Earth system models. The estimates are based on the fully coupled simulation (COU) under the 1% $yr^{-1}$ increasing CO2 experiment minus the control run to exclude model biases. Diagnostics are from years 121 to 140 (the 20 years up to quadrupling of atmospheric $CO_2$).

https://doi.org/10.5194/bg-2020-487
Preprint. Discussion started: 4 January 2021




Biogeosciences
Discussions
Open Access
EGU

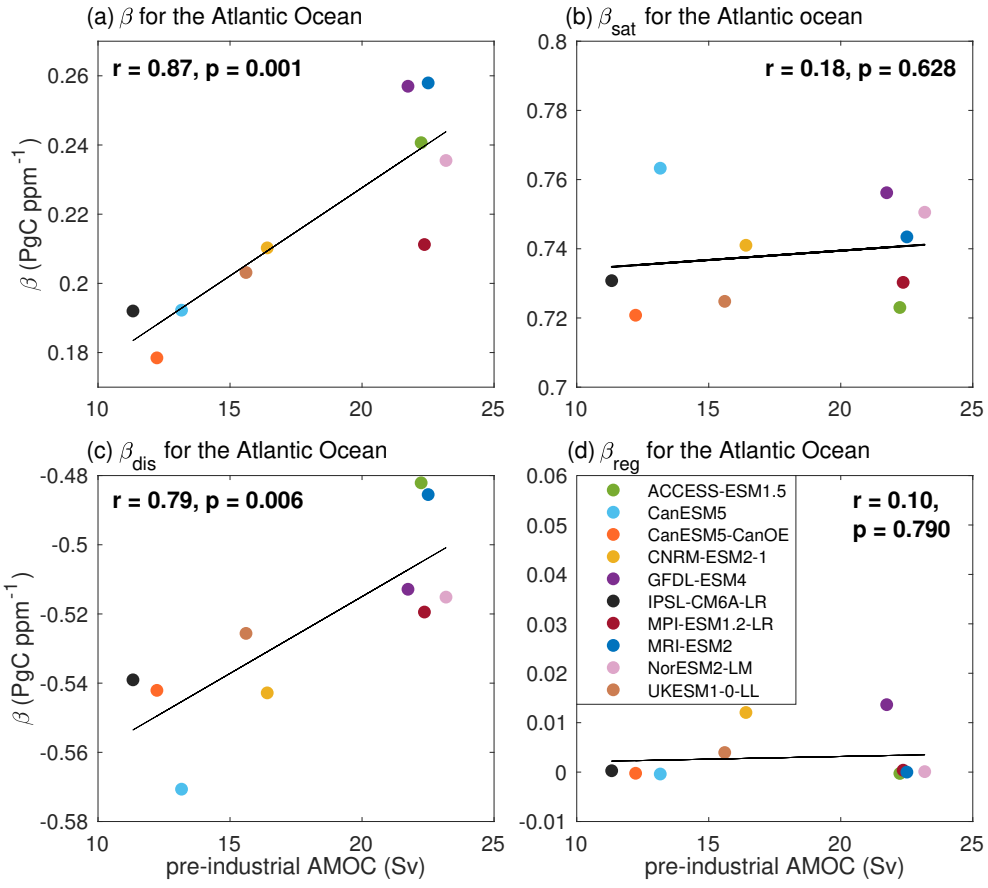


**Figure 9.** Dependence of the carbon-concentration feedback parameter, $\beta$ (PgC ppm$^{-1}$), on the pre-industrial strength of the Atlantic Meridional Overturning Circulation, AMOC ($Sv$), in the Atlantic Ocean in 10 CMIP6 models (Table 1): (a) $\beta$, (b) contribution from the saturated carbon pool, $\beta_{sat}$, (c) contribution from the disequilibrium carbon pool, $\beta_{dis}$, and (d) contribution from the regenerated carbon pool, $\beta_{reg}$. The black lines correspond to the regression line based on an ordinary least squares regression, with the corresponding correlation coefficient, $r$, and $p$-value, shown in each panel. Diagnostics are from years 121 to 140 (the 20 years up to quadrupling of atmospheric $CO_2$).

https://doi.org/10.5194/bg-2020-487
Preprint. Discussion started: 4 January 2021


Biogeosciences Discussions
Open Access
EGU

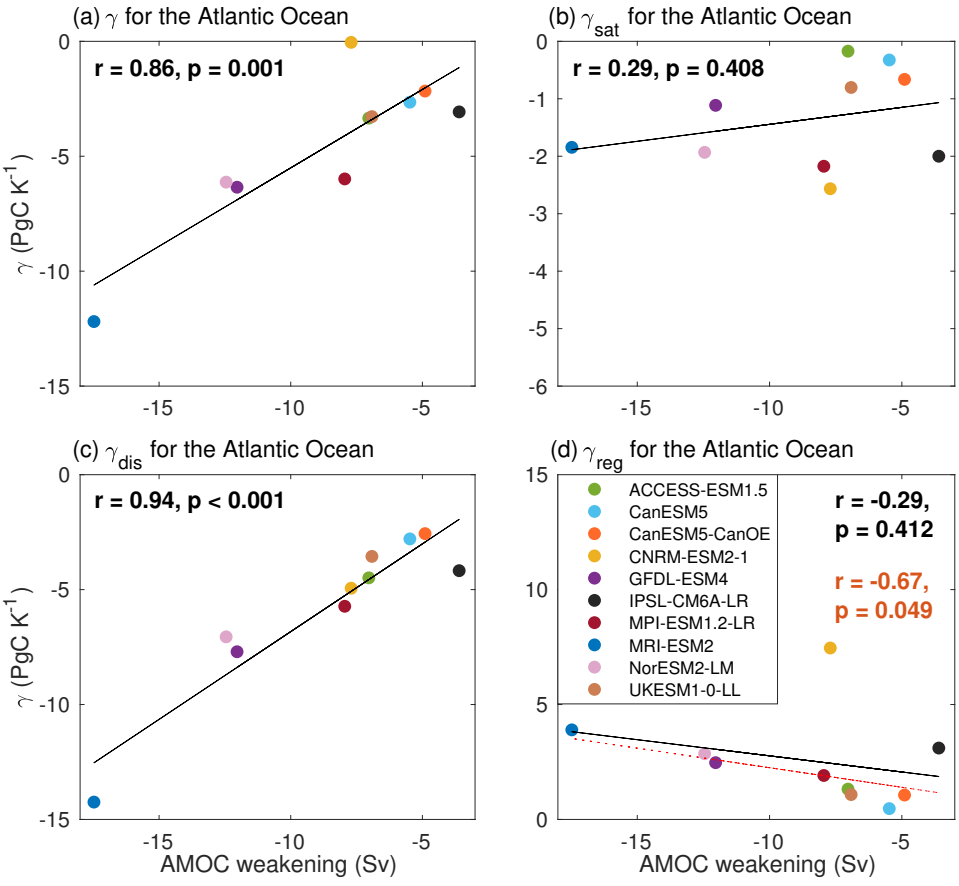


**Figure 10.** Dependence of the carbon-climate feedback parameter, $\gamma$ (PgC $K^{-1}$), on the Atlantic Meridional Overturning Circulation (AMOC) weakening with climate change in the Atlantic Ocean in 10 CMIP6 models (Table 1): (a) $\gamma$, (b) contribution from the saturated carbon pool, $\gamma_{sat}$, (c) contribution from the disequilibrium carbon pool, $\gamma_{dis}$, and (d) contribution from the regenerated carbon pool, $\gamma_{reg}$. The black lines correspond to the regression line based on an ordinary least squares regression, with the corresponding correlation coefficient, $r$, and $p$-value shown in each panel. The dashed red, line and $r$ and $p$-value in red color in (d) correspond to the regression line and the correlation coefficient estimated by excluding CNRM-ESM2-1, the model with the largest deviation from the rest of the Earth system models in terms of the regenerated carbon pool. Diagnostics are from years 121 to 140 (the 20 years up to quadrupling of atmospheric $CO_2$).

https://doi.org/10.5194/bg-2020-487
Preprint. Discussion started: 4 January 2021


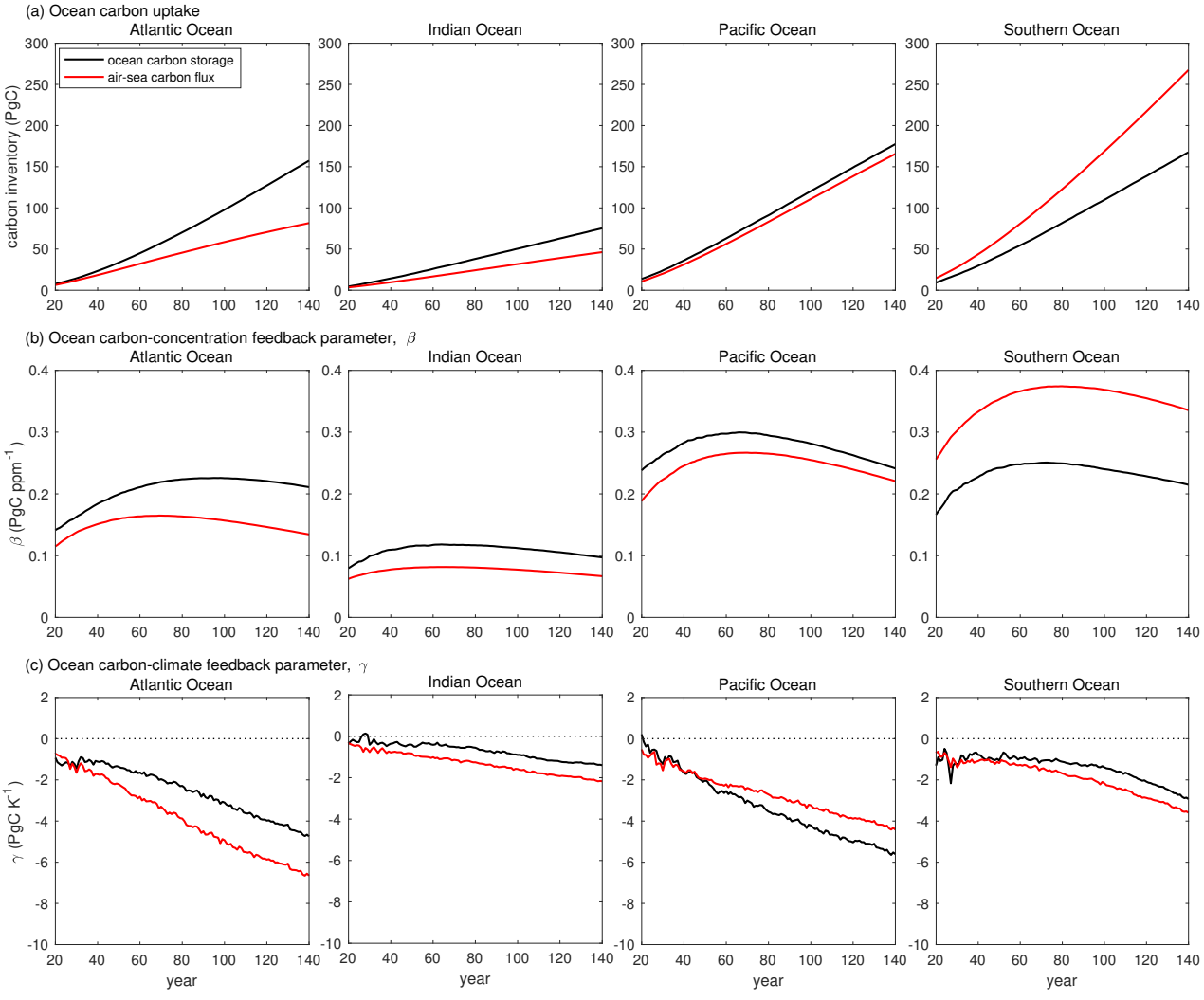


**Figure A1.** Ocean carbon storage and cumulative air-sea carbon flux in the Atlantic, Pacific, Indian and Southern Oceans in CMIP6 Earth system models, and their contribution to the ocean carbon cycle feedback parameters: (a) changes in the ocean carbon storage relative to the pre-industrial and cumulative ocean carbon uptake in PgC, (b) carbon-concentration feedback parameter, $\beta$ in PgC ppm$^{-1}$, estimated based on the ocean carbon storage and the cumulative ocean carbon uptake, and (c) carbon-climate feedback parameter, $\gamma$ in PgC K$^{-1}$, estimated based on the ocean carbon storage and the cumulative ocean carbon uptake. The black lines show the intermodel mean for the ocean carbon storage, and the red lines show the intermodel mean for the cumulative carbon uptake. The estimates are based on the fully coupled simulation (COU) and the biogeochemically coupled simulation (BGC) under the 1% yr$^{-1}$ increasing $CO_2$ experiment. The control run was used to estimate the changes relative to the pre-industrial to exclude model biases. The intermodel mean is based on the models in Table 1 excluding NorESM2-LM for which the air-sea carbon flux for the BGC run was unavailable.